Defence Research and Development Canada
Recherche et développement pour la défense Canada

DEFENCE DÉFENSE

# Linear and Second Order Keystone Transforms and Their Applications

David Kirkland

**Defence R&D Canada – Ottawa**

Canada

Technical Memorandum
DRDC Ottawa TM 2013-058
October 2013

# Linear and Second Order Keystone Transforms and Their Applications

David Kirkland
Defence R&D Canada – Ottawa

**Defence R&D Canada – Ottawa**
Technical Memorandum
DRDC Ottawa TM 2013-058
October 2013

Principal Author

*Original signed by David Kirkland*

David Kirkland

Approved by

*Original signed by Anthony Damini*

Anthony Damini
Acting Head/Radar Sensing & Exploitation Section

Approved for release by

*Original signed by Chris McMillan*

Chris McMillan
Head/Document Review Panel

# Abstract

This report covers the basic theory of the First Order (Linear) and Second Order Keystone transforms. The associated sampling requirements are then derived and two compensation methods for handling subsampled systems are discussed. Linear and Second Order Keystone transforms are then applied to the problem of imaging moving targets in Synthetic Aperture Radar (SAR) systems for both simulated and acquired data. The results show that similar performance is achieved with both Keystone based algorithms.

# Résumé

Le présent rapport porte sur les principes des transformées du trapèze de premier degré (linéaires) et de deuxième degré. Les exigences d'échantillonnage associées sont ensuite calculées et deux méthodes de traitement des systèmes sous-échantillonnés sont étudiées. Les transformées du trapèze de premier de de deuxième degré sont ensuite appliquées au problème de l'imagerie de cibles mobiles dans des systèmes de radar à synthèse d'ouverture avec des données simulées et réelles. Les résultats indiquent que les deux algorithmes à transformée du trapèze donnent des résultats similaires.

This page intentionally left blank.

# Executive summary

## Linear and Second Order Keystone Transforms and Their Applications

David Kirkland; DRDC Ottawa TM 2013-058; Defence R&D Canada – Ottawa; October 2013.

**Background:** Papers utilizing the Keystone transform and its variants have become more frequent in recent years. Unfortunately, the presentation of the mathematical properties of the Keystone based transforms often contain inconsistent mathematical notation, which can lead to confusion. Therefore, in this report the Linear and Second Order Keystone transforms are derived in a unified manner.

The Linear and Second Order Keystone transforms are valuable for imaging moving targets with translational motion in Synthetic Aperture Radar (SAR) data because they can be used to remove either the range walk or range curvature for the moving target without knowledge of its velocity. In this report, two methods of imaging moving targets are presented based on the Linear and Second Order Keystone transforms.

**Principal results:** This report presents the details of the Linear and the Second Order Keystone transforms. The sampling requirements for each of these transforms are derived, and two methods for handling subsampled data are given. The first method involves a correction factor which is applied after the Keystone transform. This approach is subject to some limitations which are described in the report. The second algorithm is more general, but involves applying a correction before the transform.

This report also details two algorithms, based on Keystone transforms, for focusing moving targets in single channel SAR systems. Results are presented for both simulated SAR data and SAR data acquired from an airborne platform. The results obtained for the two algorithms are quite similar. Although they show improved focusing of the moving target, residual smearing of the target exists which is believed to be due to limitations of the spatial Taylor series approximation, and inexact determination of the focusing parameters.

**Significance of results:** The Linear and Second Order Keystone transforms are useful tools for focusing moving targets in SAR data. They make it possible to eliminate a portion of the range migration of the target signature without prior knowledge of the target's velocity. Additional parameters must be estimated to complete the focusing procedure. The results show that the algorithms are capable of focusing most of the target signature. However residual smearing is still evident in the focused imagery. The algorithms developed in this report would need to be extended and modified to produce focused imagery of realistic targets with realistic motion characteristics such as jerk, rotational motion, and vibration.

**Future work:** The Keystone transform based algorithms described here do not perform well when the moving target signature is not sufficiently separated from that of stationary clutter. Therefore, future work should involve the study of Keystone based imaging algorithms in multi-channel systems. Such systems have additional degrees of freedom, which make it possible to suppress the stationary clutter using Space-Time Adaptive Filtering (STAP) techniques.

# Sommaire

## Linear and Second Order Keystone Transforms and Their Applications

David Kirkland ; DRDC Ottawa TM 2013-058 ; R & D pour la défense Canada – Ottawa ; octobre 2013.

**Introduction :** Les articles faisant appel à la transformée du trapèze et à ses variantes sont devenus plus fréquents ces dernières années. Malheureusement, la présentation des propriétés mathématiques des transformées du trapèze contient souvent une notation mathématique hétérogène qui peut porter à confusion. Dans le présent rapport, les transformées du trapèze de premier de de deuxième degré sont donc établies de façon façon uniforme.

Les transformées du trapèze sont utiles pour produire des images de cibles mobiles ayant un mouvement de translation à partir de données de radar à synthèse d'ouverture, car ces transformées permettent de supprimer la migration en distance (ou courbure) de la cible mobile sans connaître sa vitesse. Dans le présent rapport, deux méthodes d'imagerie des cibles mobiles sont présentées, la première faisant appel à transformée linéaire et la seconde à la transformée de deuxième degré.

**Résultats principaux :** Le présent rapport donne une description détaillée des transformées du trapèze de premier de de deuxième degré. Les exigences d'échantillonnage pour chacune de ces deux transformées sont établies et deux méthodes de traitement des données sous-échantillonnées sont indiquées. La première méthode fait appel à un facteur de correction qui est appliqué après la transformée du trapèze. Cette approche comporte certaines limites qui sont décrites dans le rapport. Le second algorithme est plus général, mais il nécessite l'application d'une correction avant la transformée.

Le présent rapport propose également deux algorithmes fondés sur les transformées du trapèze pour focaliser les cibles mobiles dans les systèmes de SAR à un seul canal. Des résultats pour des données de SAR simulées et des données de SAR acquises à partir d'une plateforme aérienne sont présentés. Les résultats obtenus pour les deux algorithmes sont assez semblables. Même s'ils fournissent une image plus nette de la cible mobile, les algorithmes ne parviennent pas à éliminer complètement le flou, ce qui semble être attribuables aux limites de l'approximation spatiale par série de Taylor ainsi qu'à la détermination inexacte des paramètres de focalisation.

**Portée des résultats :** Les transformées du trapèze de premier et de deuxième degré sont des outils utiles pour focaliser des cibles mobiles dans les données de SAR.

Elles permettent d'éliminer en partie la migration en distance de la signature de la cible sans connaître à priori la vitesse de la cible. D'autres paramètres doivent être évalués pour compléter la procédure de focalisation. Les résultats indiquent que les algorithmes sont capables de focaliser la plus grande partie de la signature de la cible, mais qu'il reste un flou résiduel dans les images focalisées. Les algorithmes proposés dans le présent rapport doivent être augmentés et modifiés pour produire des images nettes de cibles réalistes ayant des caractéristiques de mouvement réalistes, comme des mouvements de secousses, de rotation et de vibration.

**Recherches futures :** Les algorithmes fondés sur les transformées du trapèze présentés ici ne donnent pas de bons résultats lorsque la signature de la cible mobile n'est pas assez séparée de celle du fouillis stationnaire. Les recherches futures devraient donc comprendre l'étude des algorithmes d'imagerie à transformée du trapèze dans des systèmes à canaux multiples, qui ont des degrés de liberté supplémentaires permettant de supprimer le fouillis stationnaire au moyen de techniques de filtrage par traitement adaptatif espace-temps (STAP, de l'anglais Space-Time Adaptive Filtering).

# Table of contents

# List of figures

This page intentionally left blank.

# 1 Introduction

In [1], Perry et al. presented the Linear Keystone transform, which can be used to remove the range walk component of range migration without explicit knowledge of the radial velocity of the target being imaged. Later, Zhou et al., [2], developed the Second Order Keystone transform, which is capable of removing the quadratic or range curvature component of the range migration These Keystone transforms can be used to form a key component of the algorithms for focusing moving target signatures in Synthetic Aperture Radar (SAR) imagery. After application of the Keystone transform, additional range migration correction is often required and the formation of the azimuth compression filter is necessary to properly focus the moving targets.

This report introduces the Linear and Second Order Keystone transforms in a general context and analyzes the corresponding sampling requirements. Techniques for handling subsampled target signatures are derived and their limitations are discussed. The effect of moving targets with translational motion in Spotlight mode SAR imagery is derived. Two algorithms for focusing moving target signatures which utilize the Keystone transforms are described and compared.

## 1.1 Mathematical Notation

In this report we deal with signals in both temporal and spatial dimensions. For a temporal signal, the variables $t$ , and $\omega$ denote time and its Fourier counterpart temporal frequency. The units of $t$ , and $\omega$ are seconds and radians/second respectively. The temporal Fourier transform of a signal $s(t)$ is denoted as $S(\omega)$ where,

$$\begin{aligned} S(\omega) &= \mathcal{F}_t[s(t)] \\ &= \int_{-\infty}^{\infty} s(t)\exp(-j\omega t)\,d\,t. \end{aligned} \tag{1}$$

The inverse temporal Fourier transform of a signal $S(\omega)$ is identified as

$$\begin{aligned} s(t) &= F_{\omega}^{-1}\left[S(\omega)\right] \\ &= \frac{1}{2\pi}\int_{-\infty}^{\infty} S(\omega)\exp(j\omega t)\,d\,\omega. \end{aligned} \tag{2}$$

For convenience, we define the wavenumber, $k$, as

$$k = \frac{\omega}{c}, \tag{3}$$

where $c$ is the speed of light. The unit of $k$ is radians/meter.

For signals in the spatial domain $u$, the Fourier counterpart is spatial frequency, $k_u$, which is also called the wavenumber. The units of $u$ and $k_u$ are meters and radians per meter respectively. The forward Fourier transform of a spatial domain signal, $g(u)$, is denoted as $G(k_u)$, where

$$\begin{aligned} G(k_u) &= \mathcal{F}_u[g(u)] \\ &= \int_{-\infty}^{\infty} g(u) \exp(-jk_u u)\, d\, u. \end{aligned} \tag{4}$$

The inverse spatial Fourier transform of a signal $G(k_u)$ is identified as

$$\begin{aligned} g(u) &= F_{k_u}^{-1}\left[G(k_u)\right] \\ &= \frac{1}{2\pi} \int_{-\infty}^{\infty} G(k_u) \exp(jk_u u)\, d\, k_u. \end{aligned} \tag{5}$$

For convenience, we will use the symbol $\rightleftharpoons$ to denote a Fourier transform pair, that is,

$$s(t) \rightleftharpoons S(\omega), \tag{6}$$

$$g(u) \rightleftharpoons G(k_u). \tag{7}$$

# 2 Keystone Transforms

Prior to discussing the Keystone transforms the basic signal model for the radar received signal is presented. Let $g(t)$ denote the basebanded transmitted pulse. Then the pulse transmitted by the radar has the form

$$s_{xmit}(t) = g(t)\exp(j\omega_0 t), \tag{8}$$

where $t$ denotes the fast time variable and $\omega_0$ denotes the radar centre frequency. After basebanding, the received pulse has the following form

$$\begin{aligned} s_r(t,u) &= g\left(t - \frac{2R(u)}{c}\right)\exp\left(-j\omega_0\frac{2R(u)}{c}\right) \\ &= g\left(t - \frac{2R(u)}{c}\right)\exp\left(-j2k_0R(u)\right) \end{aligned} \tag{9}$$

where $u$ denotes the radar cross-range position, $R(u)$ is the instantaneous distance of the target from the radar as a function of the radar cross-range position, and $k_0 = \omega_0/c$ is the wavenumber corresponding to the radar centre frequency. Taking the Fourier transform w.r.t. the fast time variable gives

$$S_r(\omega,u) = G(\omega)\exp\left(-j2(k+k_0)R(u)\right) \tag{10}$$

where $\omega$ is the frequency variable corresponding to the fast time variable and $k = \omega/c$ is the wavenumber. After performing pulse compression on (10) the resulting signal is denoted by $S(\omega,u)$ and is given by

$$\begin{aligned} S(\omega,u) &= |G(\omega)|^2\exp\left(-j2(k+k_0)R(u)\right) \\ &= P(\omega)\exp\left(-j2(k+k_0)R(u)\right), \end{aligned} \tag{11}$$

where $P(\omega) = |G(\omega)|^2$ denotes the Fourier transform of the pulse compressed envelope. Taking the inverse Fourier transform w.r.t. the fast time frequency variable gives

$$s(t,u) = p\left(t - \frac{2R(u)}{c}\right)\exp(-j2k_0R(u)), \tag{12}$$

where $p(t)$ is the inverse Fourier transform of $P(\omega)$.

## 2.1 Linear Keystone Transformation

As shown in (11) , the basebanded range compressed signal can be written as

$$S(\omega,u) = P(\omega)\exp\left(-j2(k+k_0)R(u)\right). \tag{13}$$

Expanding $R(u)$ in a Taylor series around $u = 0$ gives:

$$R(u) = r + \dot{r}u + \frac{\ddot{r}}{2}u^2 + \ldots, \tag{14}$$

where $r = R(0)$, $\dot{r} = \left.\frac{dR(u)}{du}\right|_{u=0}$, $\ddot{r} = \left.\frac{d^2R(u)}{du^2}\right|_{u=0}$, etc. Substituting (14) into (13) gives

$$S(\omega, u) = P(\omega)\exp\left(-j2(k + k_0)[r + \dot{r}u + \phi_1(u)]\right), \tag{15}$$

where $\phi_1(u)$ denotes the quadratic and higher order terms of the Taylor series expansion.

In this and subsequent sections which discuss the Linear and Second Order Keystone transforms the Taylor series expansion of $R(u)$ is utilized. Using the variables $r$, $\dot{r}$, and $\ddot{r}$ from the Taylor series keeps the mathematical development general in nature and it is believed that this clarifies the presentation of the various Keystone transforms and their related properties. In Section 4, where we address moving targets in SAR systems, $R(u)$ is dependent on several variables such as platform position, platform velocity, target position, and target velocity. At that time it is more instructive to explicitly expand $r$, $\dot{r}$, and $\ddot{r}$ in terms of these other variables.

The Linear Keystone transform of the signal $S(\omega, u)$ is identified as $S_{k1}(\omega, u)$, where

$$S_{k1}(\omega, u) = S\left(\omega, \frac{k_0}{k + k_0}u\right). \tag{16}$$

Applying the Linear Keystone transform to (15) gives

$$\begin{aligned} S_{k1}(\omega, u) &= P(\omega)\left(\exp -j2\left[(k + k_0)r + (k + k_0)\dot{r}\frac{k_0}{k + k_0}u + \phi_{1k}(u)\right]\right) \\ &= P(\omega)\exp\left(-j2\left[(k + k_0)r + \dot{r}k_0u + \phi_{1k}(u)\right]\right), \end{aligned} \tag{17}$$

where

$$\phi_{1k}(u) = (k + k_0)\phi_1\left(\frac{k_0}{k + k_0}u\right). \tag{18}$$

Examination of (17) reveals that the range walk component of the target signature has been eliminated at the expense of increased complexity in the higher order phase terms. The advantage of applying the Linear Keystone transform is that explicit knowledge of the target radial velocity is not required in order to eliminate the effect of range walk.

To illustrate the Linear Keystone transformation, a simulated data set was generated with the parameters listed in Table 1. To clearly demonstrate the effect of the

Table 1: Simulation Parameters

| Symbol | Description | Value |
|---|---|---|
| $f_0$ | Centre Frequency | 1.0 GHz |
| PRF | Pulse Repetition Frequency | 2000 Hz |
| BW | Pulse Bandwidth | 30 MHz |
| N | Number of Pulses | 512 |
| $r$ | Initial Range | 17.55 km |
| $\dot{r}$ | Radial Velocity | 120 m/s |
| $\ddot{r}$ | Radial Acceleration | -350 m/s$^2$ |

Keystone transform the radar platform is kept stationary and the target moves radially with respect to the radar. Keeping the radar platform stationary eliminates the range migration due to the motion of the radar platform. Consequently, any range migration is due completely to the motion of the target itself. Figure 1 shows the amplitude of the target signature in the range/cross-range domain after range compression. The motion of the target includes both linear (range walk) and quadratic (range curvature) components. Figure 2 illustrates the results after application of the Linear Keystone transform. As seen in the figure, the linear component of the range migration has been removed, leaving the residual range curvature.

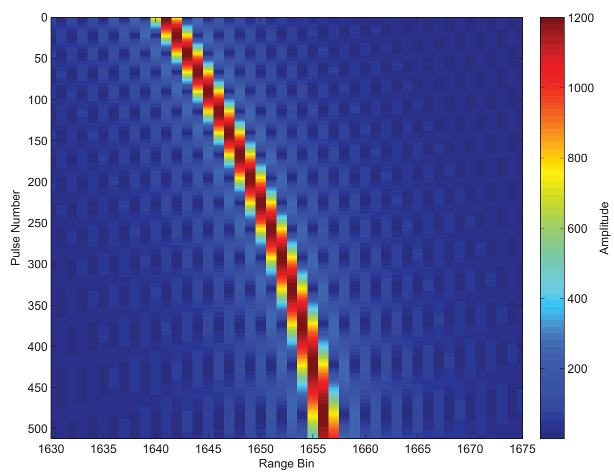


Figure 1: Range compressed target response.

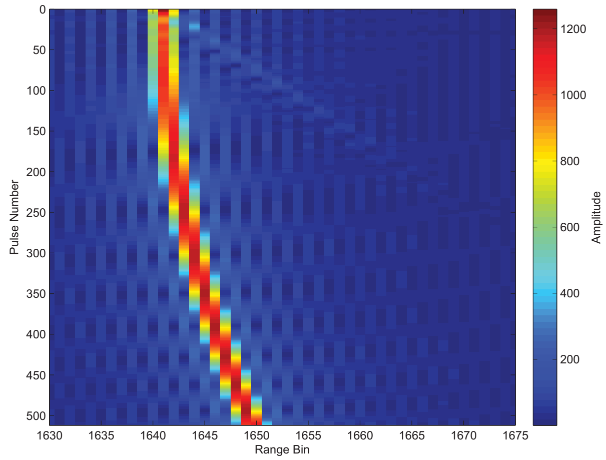


Figure 2: Target signature after application of the Linear Keystone transform.

## 2.2 Second Order Keystone Transformation

The Second Order Keystone transform of the signal $S(\omega, u)$ is identified as $S_{k2}(\omega, u)$, where

$$S_{k2}(\omega, u) = S\left(\omega, \left(\frac{k_0}{k + k_0}\right)^{\frac{1}{2}} u\right) \tag{19}$$

To examine the properties of this transform we begin by restating (15), except that now the second order terms of the Taylor series are explicitly included to give

$$\begin{aligned} S(\omega, u) &= P(\omega) \exp\left(-j2(k + k_0)R(u)\right) \\ &= P(\omega) \exp\left( - j2(k + k_0)\left[r + \dot{r}u + \frac{\ddot{r}}{2}u^2 + \phi_2(u)\right]\right), \end{aligned} \tag{20}$$

where $\phi_2(u)$ includes the cubic and higher order terms of the Taylor series expansion. Applying the Second Order Keystone transform to (20) gives

$$S_{k2}(\omega, u) = P(\omega) \exp\left(-j2\left[(k + k_0)r + \dot{r}k_0^{\frac{1}{2}}(k + k_0)^{\frac{1}{2}}u + \frac{\ddot{r}}{2}k_0 u^2 + \phi_{2k}(u)\right]\right), \tag{21}$$

where

$$\phi_{2k}(u) = (k + k_0)\phi_2\left(\left(\frac{k_0}{k + k_0}\right)^{\frac{1}{2}} u\right). \tag{22}$$

Examination of the phase of the complex exponential in (21) shows that the range curvature component has been removed. In order to clarify the significance of the second phase term, it is expanded in a Taylor series w.r.t. $k$ about the wavenumber

$k_0$, to give

$$
\begin{aligned}
k_0^{\frac{1}{2}}(k_0+k)^{\frac{1}{2}} &= k_0\left(1+\frac{k}{k_0}\right)^{\frac{1}{2}} \\
&\approx k_0\left(1+\frac{k}{2k_0}\right),
\end{aligned}
\tag{23}
$$

where higher order terms in the Taylor series have been neglected. Substituting (23) into (21) results in

$$
S_{k2}(\omega,u) \approx P(\omega)\exp\left(-j2\left[(k+k_0)r+\dot{r}\left(k_0+\frac{k}{2}\right)u+\frac{\ddot{r}}{2}k_0u^2+\phi_{2k}(u)\right]\right). \tag{24}
$$

Examination of (24) reveals that in addition to the removal of the range curvature the Second Order Keystone transform reduces the range walk by a factor of 1/2.

It should be noted that the approximation used in (23) is only used to demonstrate the effect of the Second Order Keystone transform on the range migration. For algorithms which involve further manipulation of the range walk component, the full non-linear expression in (21) should be used.

Utilizing the same simulated data set from the previous section, Figure 3 presents the result in the range/cross-range domain after the application of the Second Order Keystone transform to the range compressed data. It can be seen in the figure that only a linear component of the range migration remains. To demonstrate the factor of 1/2 reduction in the range walk component, Figure 4 presents the original simulated target signature with the radial acceleration now set to zero. Setting the radial acceleration to zero means that the range migration of the target signature only has a linear component i.e. range walk. By comparing Figures 3 and 4 it can be seen that the range walk has been reduced by a factor of 1/2 as predicted.

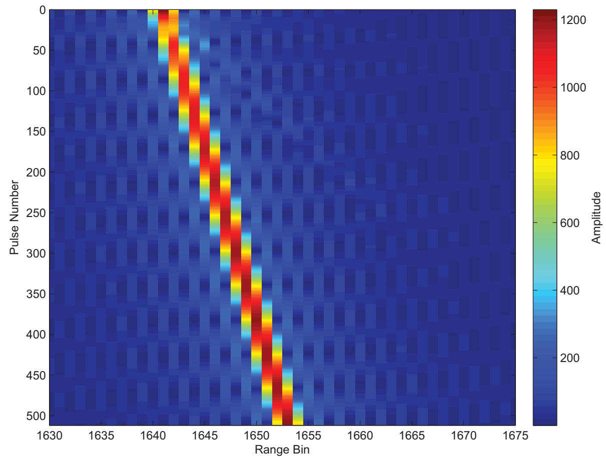


Figure 3: Target response after application of the Second Order Keystone transform.

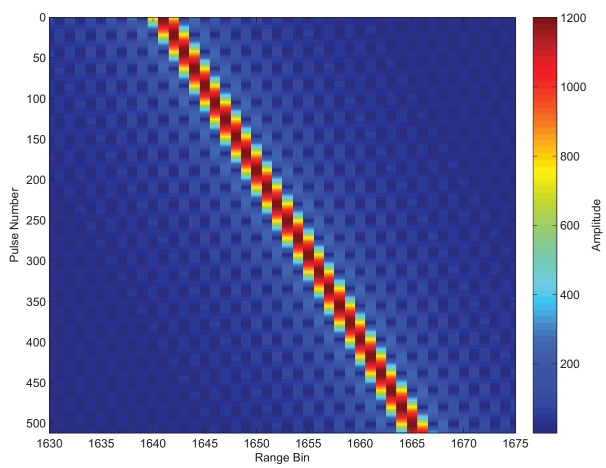


Figure 4: Range walk of target (acceleration = 0).

# 3 Sampling Related Requirements for the Keystone Transforms

This section examines the sampling related requirements associated with the Keystone transforms. The scaling of the cross-range variable in the Keystone transforms affects the spatial frequency bandwidth of the resulting signal. This impact on the bandwidth has implications on the cross-range sampling rate to ensure that the signal is adequately sampled according to the Nyquist criterion. Also addressed in this section is the situation when the target signature is subsampled in the spatial frequency domain i.e. when the cross-range sampling rate is sufficient to support the spatial frequency bandwidth of the signal, but the centre frequency of the signal lies outside of the baseband area. The requirements on the cross-range sampling rate are derived in Section 3.1. Sections 3.2 and 3.3 address the subsampling of the moving target signal in the cross-range direction.

## 3.1 Frequency Dilation

The application of a dilation factor in the cross-range dimension affects the frequency content of the received signal in the associated frequency domain. The scaling property of the Fourier transform states that if $g(u) \rightleftharpoons G(k_u)$ then

$$g(au) \rightleftharpoons \frac{1}{|a|} G\left(\frac{k_u}{a}\right), \tag{25}$$

where $a$ is a scalar dilation factor. Thus, when the cross-range variable is scaled, the spatial frequency variable is scaled in an inverse manner. To illustrate this point, Figure 5 shows an example function $G(k_u)$ and Figure 6 shows the corresponding scaled function $G(k_u/2)$ i.e. when $a = 2$. In this example, the spatial frequency bandwidth of the resulting signal has doubled and the sampling rate of the corresponding spatial domain signal would need to be adjusted appropriately to avoid aliasing.

If the bandwidth of the signal in the spatial frequency domain is given by $k_{u\_BW}$ and $\Delta u$ denotes the spacing of the spatial samples, then in order to satisfy the Nyquist criterion

$$\Delta u < \frac{2\pi}{k_{u\_BW}}. \tag{26}$$

After application of the dilation factor, $a$, to the cross-range variable, $u$, the Nyquist criterion implies that the new spacing of the spatial samples, $\Delta u'$, must satisfy

$$\Delta u' < \frac{1}{a}\frac{2\pi}{k_{u\_BW}}. \tag{27}$$

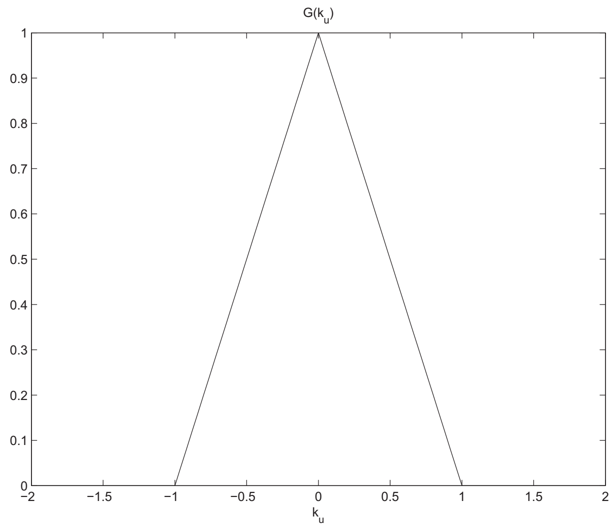


Figure 5: Original function $G(k_u)$.

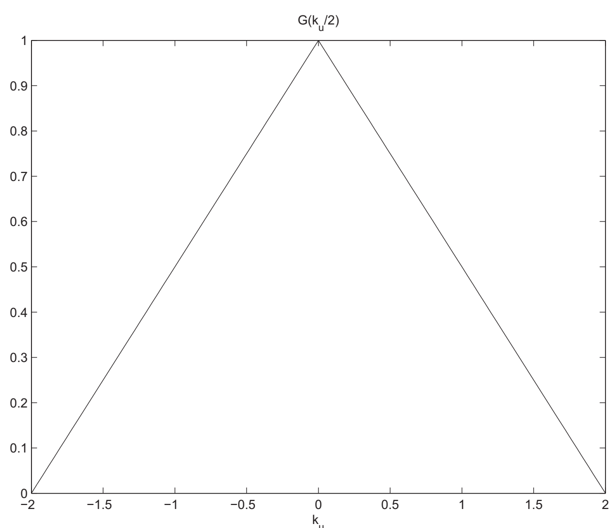


Figure 6: Scaled Function $G(k_u/2)$.

For the Linear and Second Order Keystone transforms the scaling factor is dependent on the fast time frequency variable. The overall sampling requirement is then determined by the dilation factor which results in the largest spatial frequency bandwidth. For the Linear Keystone transform the limit is given by

$$\Delta u' < \frac{1}{\max\limits_{k}\left[\frac{k_0}{k+k_0}\right]} \frac{2\pi}{k_{u\_BW}}. \tag{28}$$

Similarly, for the Second Order Keystone transform the limit is given by

$$\Delta u' < \frac{1}{\max\limits_{k}\left[\left(\frac{k_0}{k+k_0}\right)^{\frac{1}{2}}\right]} \frac{2\pi}{k_{u\_BW}}. \tag{29}$$

## 3.2 Frequency Subsampling - Case 1

This section addresses the situation when the moving target signature is subsampled i.e. when the target has a radial velocity such that the target is "aliased" in the spatial frequency domain. Consider a target with only a radial velocity, then (15) can be rewritten as

$$S(\omega, u) = P(\omega) \exp\left(-j2(k+k_0)[r + \dot{r}u]\right). \tag{30}$$

Taking the partial derivative of the phase w.r.t. $u$ gives the instantaneous spatial Doppler frequency, $k_u$, as

$$k_u = -2(k+k_0)\dot{r}. \tag{31}$$

Given the cross-range sample spacing of $\Delta u$ meters, aliasing of the spatial Doppler frequency will occur if

$$\begin{aligned} |k_u| &> \frac{k_s}{2} \\ &> \frac{\pi}{\Delta u}, \end{aligned} \tag{32}$$

where $k_s = 2\pi/\Delta u$ is the spatial Doppler sampling frequency in rad/m.

In this case, the spatial Doppler frequency can be represented as

$$k_u = k_b + N k_s, \tag{33}$$

where $|k_b| < k_s/2$ represents the aliased result of the subsampled spatial Doppler frequency $k_u$, and $N$ is an integer and represents the foldover factor. Essentially (33) divides the spatial Doppler frequency domain into bands each having a bandwidth of

$k_s$. A different band is associated with each value of $N$. Equating (31) and (33) and solving for $\dot{r}$ gives

$$\dot{r} = -\frac{k_b + Nk_s}{2(k + k_0)}. \tag{34}$$

Substituting (34) into (30) gives

$$\begin{aligned}
S(\omega, u) &= P(\omega) \exp\left(-j2(k + k_0)\left[r - \frac{k_b + Nk_s}{2(k + k_0)}u\right]\right) \\
&= P(\omega) \exp\left(-j2(k + k_0)r + jk_b u + jNk_s u\right) \\
&= P(\omega) \exp\left(-j2(k + k_0)r + jk_b u + jN\frac{2\pi}{\Delta u}M\Delta u\right) \\
&= P(\omega) \exp\left(-j2(k + k_0)r + jk_b u\right),
\end{aligned} \tag{35}$$

where we have utilized the relationships that $u = M\Delta u$, where $M$ is an integer, and $k_s = 2\pi/\Delta u$.

Applying the Linear Keystone transform to the subsampled signal (35) gives

$$S_{k1}(\omega, u) = P(\omega) \exp\left(-j2(k + k_0)r + jk_b\frac{k_0}{k + k_0}u\right), \tag{36}$$

Solving (34) for $k_b$

$$k_b = -2(k + k_0)\dot{r} - Nk_s \tag{37}$$

and substituting (37) into (36) gives

$$\begin{aligned}
S_{k1}(\omega, u) &= P(\omega) \exp\left(-j2(k + k_0)r - j2(k + k_0)\dot{r}\frac{k_0}{k + k_0}u - jNk_s\frac{k_0}{k + k_0}u\right) \\
&= P(\omega) \exp\left(-j2(k + k_0)r - j2\dot{r}k_0 u - jNk_s\frac{k_0}{k + k_0}u\right).
\end{aligned} \tag{38}$$

Examination of (38) reveals that $S_{k1}(\omega, u)$ contains an additional phase term which produces an uncompensated range migration component. To eliminate this undesired range migration component from (38) requires multiplication by the factor $\exp\left(j\frac{Nk_s k_0}{k+k_0}u\right)$. We therefore define the corrected signal, $\tilde{S}_{k1}(\omega, u)$, as

$$\begin{aligned}
\tilde{S}_{k1}(\omega, u) &= \exp\left(j\frac{Nk_s k_0}{k + k_0}u\right) S_{k1}(k, u) \\
&= P(\omega) \exp\left(-j2(k + k_0)r - j2\dot{r}k_0 u\right).
\end{aligned} \tag{39}$$

An analysis similar to this one can be conducted to develop a correction for the application of the Second Order Keystone transform to a subsampled signal. Applying the Second Order Keystone transform to the subsampled signal (35) gives

$$S_{k2}(\omega,u) = P(\omega)\exp\left(-j2(k+k_0)r + jk_b\left(\frac{k_0}{k+k_0}\right)^{\frac{1}{2}} u\right). \tag{40}$$

Substituting (37) into (40) gives

$$\begin{aligned} S_{k2}(\omega,u) &= P(\omega)\exp\left(-j2(k+k_0)r - j2(k+k_0)\dot{r}\left(\frac{k_0}{k+k_0}\right)^{\frac{1}{2}} u - jNk_s\left(\frac{k_0}{k+k_0}\right)^{\frac{1}{2}} u\right) \\ &= P(\omega)\exp\left(-j2(k+k_0)r - j2\dot{r}\left(k_0(k+k_0)\right)^{\frac{1}{2}} u - jNk_s\left(\frac{k_0}{k+k_0}\right)^{\frac{1}{2}} u\right). \end{aligned} \tag{41}$$

Examination of (41) reveals that $S_{k2}(\omega,u)$ contains an additional phase term, caused by the subsampling of the Second Order Keystone transform which will produce undesired range migration. To correct for the additional range migration term after application of the Second Order Keystone transform requires multiplication by the factor $\exp\left(jNk_s\left(\frac{k_0}{k+k_0}\right)^{\frac{1}{2}} u\right)$. For the Second Order Keystone transform we define the corrected signal, $\tilde{S}_{k2}(\omega,u)$, as

$$\begin{aligned} \tilde{S}_{k2}(\omega,u) &= \exp\left(jNk_s\left(\frac{k_0}{k+k_0}\right)^{\frac{1}{2}} u\right) S_{k2}\left(\omega,u\right). \\ &= P(\omega)\exp\left(-j2(k+k_0)r - j2\dot{r}\left(k_0(k+k_0)\right)^{\frac{1}{2}} u\right). \end{aligned} \tag{42}$$

To simplify the preceding analysis, it was assumed that the radial acceleration of the target was zero. It should be noted that the same modulation correction derived above can also be applied to the situation when the target possesses radial acceleration. For the modulation correction to be applicable, the constraint (33) still applies. This requires that the spatial Doppler bandwidth of the moving target signal is less than $k_s$ and that the spatial Doppler frequency of the target does not traverse from one spatial Doppler band into another.

To demonstrate the effect of the phase correction given in (39) and (42) we create a simulation scenario where the moving target signal is subsampled and satisfies the condition in (33). Table 2 lists the radar and target parameters used in the following simulation. Figure 7 shows the amplitude of the range compressed data in the range/cross-range domain for this target. Figure 8 depicts the results after application of the Linear Keystone transform. The target signature in Figure 8 still contains a large range walk component. Figure 9 illustrates the results after applying

Table 2: Simulation Parameters

| Symbol | Description | Value |
|---|---|---|
| $f_0$ | Centre Frequency | 1.0 GHz |
| PRF | Pulse Repetition Frequency | 2000 Hz |
| BW | Pulse Bandwidth | 30 MHz |
| N | Number of Pulses | 512 |
| $r$ | Initial Range | 17.55 km |
| $\dot{r}$ | Radial Velocity | 180 m/s |
| $\ddot{r}$ | Radial Acceleration | 350 m/s$^2$ |

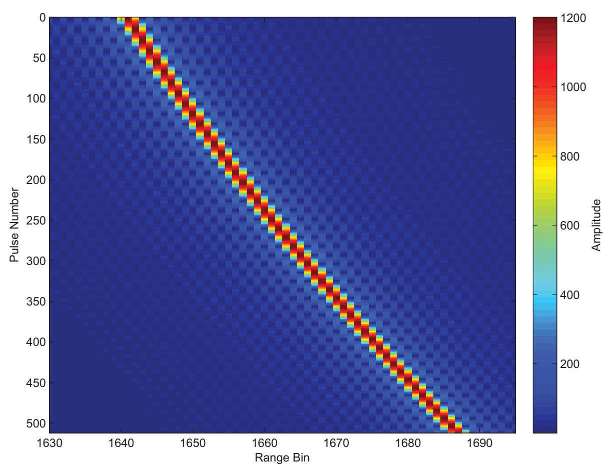


Figure 7: Range compressed target signature.

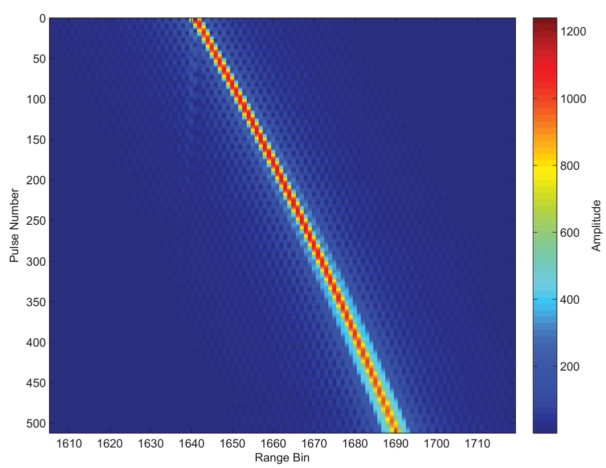


Figure 8: Range compressed target signature after application of the Linear Keystone transform.

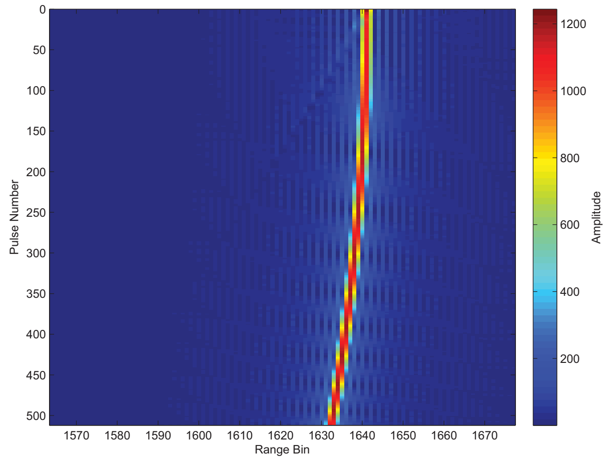


Figure 9: Range after modulation correction.

the correction given in (39). The remaining range walk component of the target signature has been removed and only residual range curvature remains.

The advantage of the corrections given in (39) and (42) is that they can be applied after the Keystone transforms. Unfortunately, there are also a couple of disadvantages. The first occurs when the velocity of the target is such that the spatial Doppler frequency is close to $k_s/2$. Due to the application of the dilation factor in the Keystone transforms the resulting signal is not uniformly sampled because the dilation factor varies as a function of the temporal frequency value. To regain uniform sample spacing requires the application of a low-pass interpolation filter in the cross-range domain. This low pass filter can result in a loss of target signal energy when the target spatial Doppler frequency falls outside the passband region of the filter. The second disadvantage occurs when the target is accelerating such that the spatial Doppler frequency moves from one spatial Doppler band into another. In this case the spatial Doppler frequency cannot be represented by (33). Section 3.3 presents an alternative approach which addresses these issues.

## 3.3 Frequency Subsampling - Case 2

In the case where the motion of the target possesses significant radial acceleration, the compensation scheme introduced in Section 3.2 can prove to be inadequate and an alternative approach is required. If we consider a moving target which only has a radial velocity ($\dot{r}$) and a radial acceleration ($\ddot{r}$), then we can rewrite (15) as

$$S(\omega, u) = P(\omega) \exp\left(-j2(k + k_0)[r + \dot{r}u + \frac{\ddot{r}}{2}u^2]\right). \tag{43}$$

The instantaneous spatial Doppler frequency, $k_u$, is obtained by taking the partial derivative of the phase w.r.t. $u$ to give

$$k_u = -2(k + k_0)\left(\dot{r} + \ddot{r}u\right). \tag{44}$$

In this case, the instantaneous spatial Doppler frequency is now dependent on the variable $u$. Due to this dependence on the cross-range position it is possible for $k_u$ to transition from one spatial Doppler band to another as the value of $u$ changes, and the instantaneous spatial Doppler frequency cannot be represented by (33). It is noted that a spatial Doppler band is defined as the spatial Doppler frequency region associated with a given value of $N$ in (33). We can rewrite (43) as

$$S(\omega, u) = P(\omega) \exp\left(-j2(k + k_0)[r + (\dot{r}_b + \dot{r}_c)u] + \frac{\ddot{r}}{2}u^2\right), \tag{45}$$

where we have let $\dot{r} = \dot{r}_b + \dot{r}_c$. Here, $\dot{r}_b$ represents a basebanded velocity such that $-k_s/2 < -2(k + k_0)\dot{r}_b < k_s/2$ and $\dot{r}_c$ represents an offset velocity. The values of $\dot{r}_b$, and $\dot{r}_c$ are yet to be determined and it is possible that multiple combinations of $\dot{r}_b$ and $\dot{r}_c$ are possible which satisfy the given conditions. If we apply a modulation function of the form $\exp(j2(k+k_0)\dot{r}_c u)$ to $S(\omega, u)$ in (45), the resulting signal $S'(\omega, u)$ is given by

$$\begin{aligned} S'(\omega, u) &= S(\omega, u) \exp(j2(k + k_0)\dot{r}_c u) \\ &= P(\omega) \exp\left(-j2(k + k_0)[r + \dot{r}_b u + \frac{\ddot{r}}{2}u^2]\right). \end{aligned} \tag{46}$$

The instantaneous spatial Doppler frequency of (46) is now obtained by taking the partial derivative of the phase w.r.t. $u$ to give

$$k_u = -2(k + k_0)\left(\dot{r}_b + \ddot{r}u\right). \tag{47}$$

If the offset velocity, $\dot{r}_c$, is chosen correctly then the spatial Doppler frequency of $S'(\omega, u)$ will fall completely within the range $-k_s/2 < k_u < k_s/2$. The Keystone transforms can then be directly applied to the modified signal $S'(\omega, u)$.

Table 3: Radar Simulation Parameters

| Symbol | Description | Value |
|---|---|---|
| $f_0$ | Centre Frequency | 1.0 GHz |
| PRF | Pulse Repetition Frequency | 2000 Hz |
| BW | Pulse Bandwidth | 30 MHz |
| N | Number of Pulses | 512 |
| $r$ | Initial Range | 17.55 km |
| $\dot{r}$ | Radial Velocity | 120 m/s |
| $\ddot{r}$ | Radial Acceleration | 350 m/s$^2$ |
| $r_c$ | Offset Velocity | 195 m/s |

The advantage of applying spatial Doppler basebanding before the Keystone transform is that this provides a very general solution. The disadvantage of this method is that an appropriate value of $\dot{r}_c$ needs to be determined. Since the Keystone transforms have to be performed for each trial value of $\dot{r}_c$ this results in an increased computational cost.

To demonstrate the effect of the modulation correction we create a simulation scenario in which the spatial Doppler frequency of the moving target signal transitions from one spatial Doppler frequency band into another. Table 3 lists the parameters for the following simulation. Figure 10 shows the amplitude of the range compressed target signature in the range/cross-range domain. Figure 11 shows the results after applying the Linear Keystone transform. In this case, it can be seen that the response of the target is split into two different segments. Figure 12 shows the results of applying the modulation correction given in (46) to the original range compressed signal data. Figure 13 shows the results of applying the Linear Keystone transform to the modulation corrected signal data. The range walk component of the target signature in Figure 13 has been removed and only a residual range curvature component remains. Comparison of Figure 11 and Figure 13 shows that the modulation correction results in a target signature which is now continuous over the pulses when the Linear Keystone transform is applied.

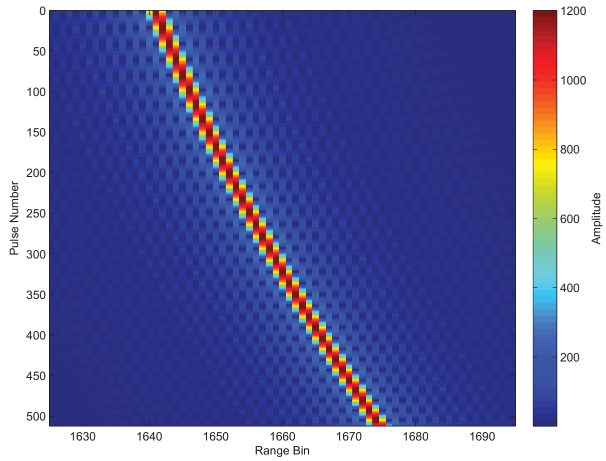


Figure 10: Range compressed target signature.

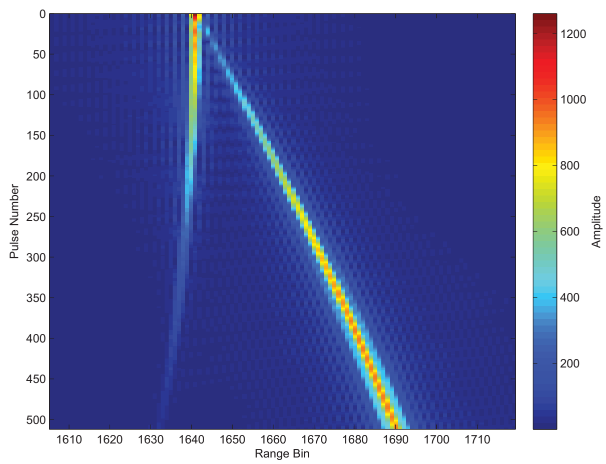


Figure 11: Target signature after applying the Linear Keystone transform.

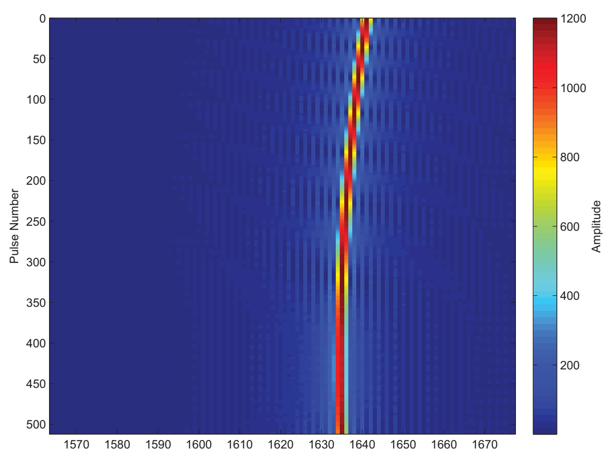


Figure 12: Range compressed target signature after modulation correction.

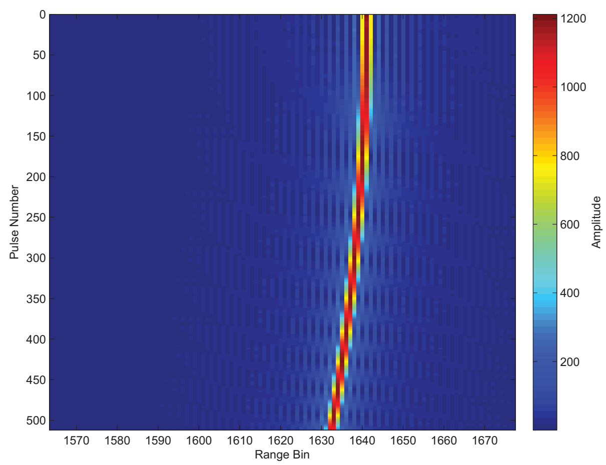


Figure 13: Result after applying the Linear Keystone transform to modulation corrected signal.

# 4 Focusing Moving Targets in Spotlight SAR

In this section two algorithms are developed for focusing moving targets in SAR data. These algorithms are based on the Keystone transforms discussed in Section 2. First the signal model for the Spotlight mode SAR is developed. Section 4.1 presents an imaging algorithm based on the Linear Keystone transform [1]. An algorithm based on the Second Order Keystone transform is developed in Section 4.2. Section 4.3 and Section 4.4 present the results of applying these algorithms to simulated data and data acquired with DRDC's X-band Wideband Experimental Airborne Radar (XWEAR) system.

The data collection geometry for the radar is shown in Figure 14. The instantaneous radar position is given by $(0, u)$. $X_c$ and $Y_c$ denote the centre of the spotlight scene in the range and cross-range directions respectively. The instantaneous position of a moving target is given by $(X_c + x_0 + v_x u, Y_c + y_0 + v_y u)$, where $x_0$ and $y_0$ denote the initial offset position of the moving target from the scene centre in the range and cross-range directions respectively. $v_x$ and $v_y$ denote the moving target's velocities in the range and cross-range directions respectively. For convenience the velocity components of the moving target have been normalized by the radar platform velocity.

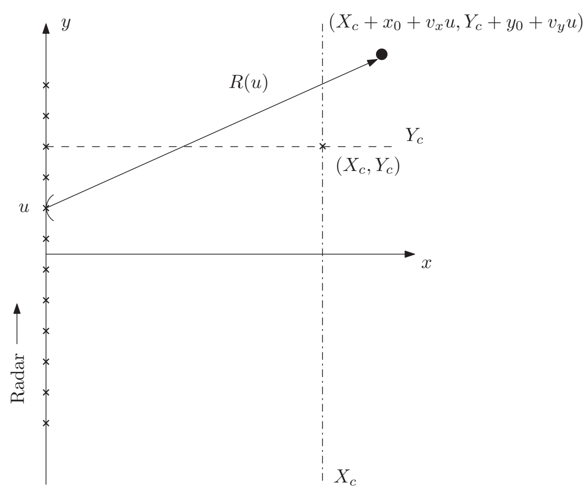


Figure 14: SAR imaging geometry.

After range compression, basebanding and motion compensation to a point, the received radar signal for the moving target, $S(\omega, u)$, in the frequency/cross-range domain can be written as

$$S(\omega, u) = P(\omega) \exp\left(j\phi(\omega, u)\right), \tag{48}$$

where

$$\phi(\omega, u) = -2(k + k_0) R_\Delta(u), \tag{49}$$

$$R_\Delta(u) = R(u) - R_{ref}(u), \tag{50}$$

$$R(u) = \left[(X_c + x_0 + v_x u)^2 + (Y_c + y_0 + v_y u - u)^2\right]^{\frac{1}{2}}, \tag{51}$$

$$R_{ref}(u) = \left[(X_c)^2 + (Y_c - u)^2\right]^{\frac{1}{2}}, \tag{52}$$

where $k = \frac{\omega}{c}$ is the wavenumber (relative to $k_0$), and $\phi(\omega, u)$ denotes the phase response of the moving target.

In Appendix A, (A.9) provides a general approximation for $R_\Delta(u)$ as:

$$\begin{aligned} R_\Delta(u) \approx & \left(\cos\theta_c + \frac{\sin\theta_c \cos\theta_c}{R_c} u\right)(x_0 + v_x u) \\ & + \left(\sin\theta_c - \frac{\cos^2\theta_c}{R_c} u\right)(y_0 + v_y u), \end{aligned} \tag{53}$$

where $\theta_c = \tan^{-1}(Y_c/X_c)$ denotes the squint angle when $u = 0$. Squint mode operation and its effect on phase is described in Appendix B, where it is shown that utilizing a rotated coordinate system allows the squint mode operation to be treated in the same manner as the broadside geometry. For the remainder of this report it is convenient to assume, without any loss of generality, that the radar operates around the point $\theta_c = 0$ i.e. broadside. This simplifies the subsequent mathematics, and (53) can then be written as

$$R_\Delta(u) = x_0 + \left(v_x - \frac{y_0}{R_c}\right) u - \frac{v_y}{R_c} u^2. \tag{54}$$

The phase response of the moving target is then obtained from (49) and (54) as

$$\begin{aligned} \phi(\omega, u) = -2(k + k_0) \Bigg[ & x_0 + \\ & + \left(v_x - \frac{y_0}{R_c}\right) u - \frac{v_y}{R_c} u^2 \Bigg]. \end{aligned} \tag{55}$$

In (55) the phase terms dependent on $k$ result in range migration i.e. range walk and range curvature, while the phase terms dependent on $k_0$ result in azimuth translation and azimuth defocusing [3]. The range velocity, $v_x$, results in a translation in the cross-range dimension of the final SAR image of the moving target. The cross-range velocity, $v_y$, introduces range curvature and cross-range smearing in the resulting SAR image of the moving target [3].

## 4.1 Focusing Algorithm Based on the Linear Keystone Transform

In this section we develop an algorithm utilizing the Linear Keystone transform to focus a moving target in SAR data[1]. We begin by applying the Linear Keystone transform to (48) and use (54) to give

$$S_{k1}(\omega, u) = P(\omega) \exp\left(j\phi_{k1}(\omega, u)\right) \tag{56}$$

where

$$\begin{aligned} \phi_{k1}(\omega, u) &= \phi\left(\omega, \frac{k_0}{k+k_0} u\right) \\ &= -2(k+k_0)x_0 - 2k_0\left(v_x - \frac{y_0}{R_c}\right)u + 2\frac{k_0^2}{k+k_0}\frac{v_y}{R_c}u^2 \end{aligned} \tag{57}$$

Examination of (57) shows that the range velocity, $v_x$, results in a shift of the moving target in the cross-range dimension of the resulting SAR image. This shift does not affect the focusing of the moving target. The cross-range velocity, $v_y$, results not only in range curvature but also in smearing of the moving target signature in the resulting SAR image. To produce a focused image of the moving target, these effects require appropriate correction.

The algorithm proposed in [1] applies trial phase corrections of the form

$$\phi_{cor}(\omega, u) = -2\frac{k_0^2}{k+k_0}\frac{\hat{v}_y}{R_c}u^2 \tag{58}$$

where $\hat{v}_y$ is an estimate of the correct cross-range velocity. After application of the correct phase correction (i.e. when $\hat{v}_y = v_y$) the resulting target signature is given by

$$\begin{aligned} S_{cor}(\omega, u) &= S_{k1}(\omega, u)\exp(j\phi_{cor}(k, u)) \\ &= P(\omega)\exp\left(-2(k+k_0)x_0 - 2k_0\left(v_x - \frac{y_0}{R_c}\right)u\right). \end{aligned} \tag{59}$$

The final image of the moving target is obtained by taking the inverse 2D FFT of $S_{cor}(\omega, u)$. The correct value of $\hat{v}_y$ is determined by selecting the value which optimizes an image quality metric such as the contrast or the brightness [1, 4].

Examination of (59) reveals that the spatial Doppler frequency in the resulting image is determined by the target's cross range position. To see this, we take the partial derivative of the phase of (59) w.r.t. $u$ to determine the instantaneous spatial Doppler frequency $k_u$ as

$$k_u = 2k_0 \frac{y_0}{R_c}, \tag{60}$$

where we have set $v_x = 0$ for convenience. If a N point inverse FFT is used in the final step of the Linear Keystone based algorithm, and the spatial sampling distance is $\Delta u$, then the spatial Doppler frequencies correspond to

$$k_{fft} = m \frac{2\pi}{N\Delta u}, \tag{61}$$

where $m$ corresponds to the FFT bin number. Equating $k_u$ and $k_{fft}$ and solving for $y_0$ gives

$$y_0 = \frac{m\pi}{k_0 N \Delta u} R_c. \tag{62}$$

The relationship given in (62) allows us to associate a cross-range pixel location in the resulting SAR image with the spatial coordinate system given in Figure 14.

## 4.2 Focusing Algorithm Based on the Second Order Keystone Transform

In this section we develop an algorithm based on the Second Order Keystone transform to focus a moving target in SAR data. We begin by applying the Second Order Keystone transform to (48) and use (54) to give

$$S_{k2}(\omega, u) = P(\omega) \exp\left(j\phi_{k2}(\omega, u)\right) \tag{63}$$

where

$$\begin{aligned} \phi_{k2}(\omega, u) &= \phi\left(\omega, \left(\frac{k_0}{k + k_0}\right)^{\frac{1}{2}} u\right) \\ &= -2(k + k_0)x_0 - 2\left(k_0(k + k_0)\right)^{\frac{1}{2}} \left(v_x - \frac{y_0}{R_c}\right) u + 2k_0 \frac{v_y}{R_c} u^2 \end{aligned} \tag{64}$$

Examination of (64) shows that the range curvature due to the cross-range velocity, $v_y$, has been removed. Range walk remains due to the range velocity, $v_x$, and cross-range smearing remains due to the cross-range velocity, $v_y$. Both of these require compensation in order to produce a focused image of the moving target. It is noted that the non-linear dependence on both $k_0$ and $k$ will also introduce higher order artifacts in the resulting SAR image. A more detailed analysis of these errors is provided in [5].

To compensate for the cross-range smearing, trial values of $\hat{v}_y$ are used in applying a phase correction of the form

$$\phi_{cor}(\omega, u) = -2k_0 \frac{\hat{v}_y}{R_c} u^2. \tag{65}$$

The resulting signal is then given by

$$\begin{aligned} S_{cor}(\omega, u) &= S_{k2}(k, u) \exp(j\phi_{cor}(\omega, u)) \\ &= P(\omega) \exp\left(j\phi_{res}(\omega, u)\right), \end{aligned} \tag{66}$$

where $\phi_{res}(\omega, u)$ is the residual phase after the phase correction. However, to be able to determine if this phase correction corresponds to the correct value of $\hat{v}_y$, the remaining range walk needs to be corrected.

When the correct value of $\hat{v}_y$ has been chosen the resulting phase, in (66), is given as

$$\begin{aligned} \phi_{res}(\omega, u) &= -2(k + k_0)x_0 - 2\left(k_0(k + k_0)\right)^{\frac{1}{2}} \left(v_x - \frac{y_0}{R_c}\right) u \\ &= -2(k + k_0)x_0 - 2\left(k_0(k + k_0)\right)^{\frac{1}{2}} \left(\frac{y_0'}{R_c}\right) u, \end{aligned} \tag{67}$$

where $\frac{y_0'}{R_c} = v_x - \frac{y_0}{R_c}$. Unfortunately, it is not possible to form a focused image of the moving target by applying a single phase correction. Instead, we build the focused target image one range line at a time, where by range line we mean a line at a constant cross-range value given by $y_i$. To produce a focused range line we apply a matched filter based on the desired value of $y_i$ in the focused SAR image. The process is then repeated at other desired values of $y_i$ to form the remaining portions of the focused imagery. This approach is similar to the range stacking algorithm described in [6], but applied here to the cross-range dimension. The focused range line, $f(t, y_i)$, is given by

$$f(t, y_i) = \mathcal{F}_\omega^{-1} \left[ \sum_u S_{cor}(\omega, u) \exp\left( j2\left(k_0(k + k_0)\right)^{\frac{1}{2}} \left(\frac{y_i}{R_c}\right) u \right) \right]. \tag{68}$$

To see that (68) produces a focused range line, we take the temporal Fourier transform of (68) and let $y_i = y_0'$ to give

$$\begin{aligned} F(\omega, y_i) &= \sum_u S_{cor}(\omega, u) \exp\left( j2\left(k_0(k + k_0)\right)^{\frac{1}{2}} \left(\frac{y_0'}{R_c}\right) u \right) \\ &= \sum_u P(\omega) \exp(-j2(k + k_0)x_0), \end{aligned} \tag{69}$$

where we have used (66). Examination of (69) shows that the summation over the cross-range variable $u$ provides coherent integration (matched filtering) when $y_i = y_0'$.

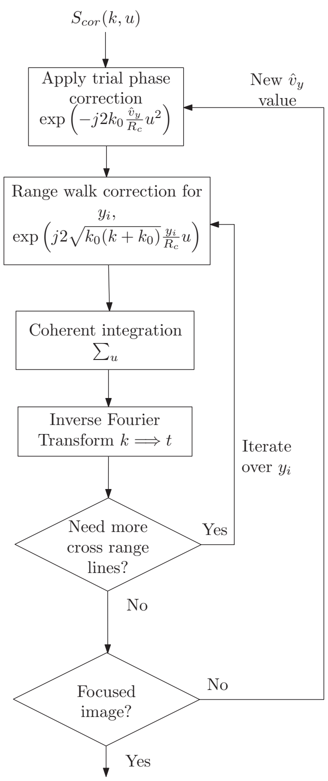


Figure 15: Second Order Keystone based focusing algorithm.

Additionally, (69) is linear w.r.t. to the values in range which allows the formation of a focused range line by taking the inverse temporal Fourier transform. Figure 15 provides a flowchart overview of the algorithm to focus a moving target. Since the range walk correction must be performed for each trial value of $\hat{v}_y$, the procedure is more computationally intensive than the Linear Keystone transform based algorithm.

In order to compare the imagery between the Linear Keystone and Second Order Keystone transform based algorithms it is useful to ensure that the images are evaluated on the same imaging grid. For example, assume that the inverse 2D FFT used to form the final image in the Linear Keystone transform based algorithm produces cross-range image samples at values of 0m , 1m, 2m, ..., then for the Second Order Keystone transform based algorithm it is necessary that we set $y_i$ = 0m , 1m, 2m, ..., as well. To ensure the alignment of the imaging grids we set the values $y_i$ equal to the values of $y_0$ determined in (62), that is,

$$y_i = \frac{m\pi}{k_0 N \Delta u} R_c. \tag{70}$$

By using these values of $y_i$ in the algorithm given in Figure 15 the output of this algorithm can be directly compared to the output of the Linear Keystone based one.

## 4.3 Imaging Results with Simulated Data

To demonstrate the ability of the two Keystone transform based algorithms to focus a moving target a simulation data set was prepared. Table 4 gives the simulation parameters. The single moving target consists of a set of point targets (elements) as shown in Figure 16. Since we are assuming the target only has translational motion, all of the elements in the target have the same velocities as those listed in Table 4. The single elements located at the near and far ranges allow examination of the variation of the point spread responses as a function of range. The seven elements distributed in cross-range across the middle of the target make it possible to evaluate the focusing capability of the algorithms.

Figure 17 shows the SAR image of the target, in the range/spatial Doppler domain, when the target is stationary. This provides a reference image for comparison of the results of the imaging algorithms for the moving target. Figure 18 shows the resulting SAR image when the target is moving with the range and cross-range velocities listed in Table 4. No processing has been applied to correct for the target motion. The resulting range curvature and cross-range smearing due to the target motion are readily apparent in this image.

Figure 19 shows the results after applying the Linear Keystone based algorithm described in Section 4.1. The figure shows the focusing of the individual elements which make up the moving target signature, in particular the seven elements spaced in the cross-range direction. The focused target response displays some residual smearing. This is believed to occur for several reasons: spatial limitation of the Taylor series expansion (see Appendix A), implementation of the interpolation procedure, and inexact determination of the target velocity.

Figure 20 shows the results after applying the Second Order Keystone based algorithm described in Section 4.2. The figure shows very similar results to those for the algorithm based on the Linear Keystone transform. The moving target response

Table 4: Simulation Parameters

| Symbol | Description | Value |
|---|---|---|
| PRF | Pulse Repetition Frequency | 400 Hz |
| $f_0$ | Centre Frequency | 9.5 GHz |
| $R_c$ | Range to Scene Centre | 19 km |
| $BW$ | Pulse Bandwidth | 600 MHz |
| $\theta_c$ | Squint Angle | 20° |
| $v_p$ | Platform Velocity | 150 m/s |
| $v_x$ | Target cross-range velocity | 8.2 m/s |
| $v_y$ | Target Radial velocity | -22.55 m/s |

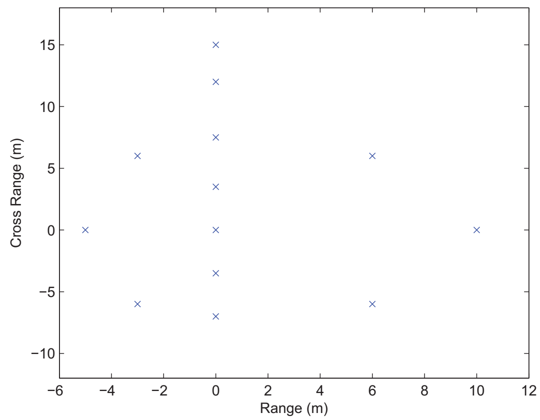


Figure 16: Simulated target configuration.

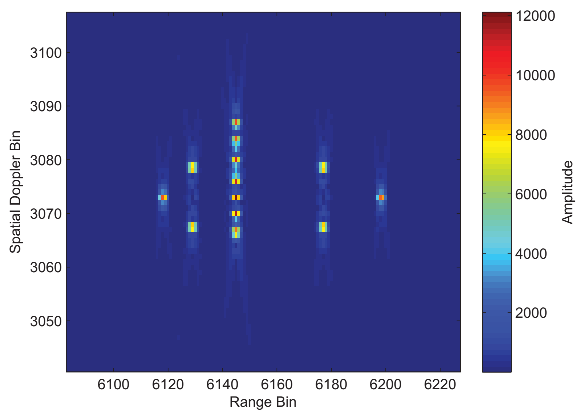


Figure 17: SAR image of non-moving target.

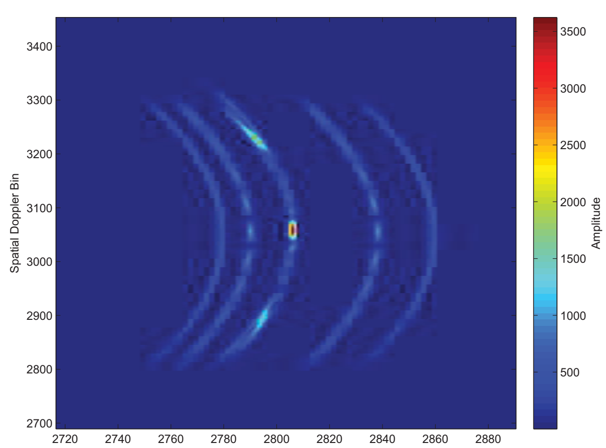


Figure 18: SAR image of moving target.

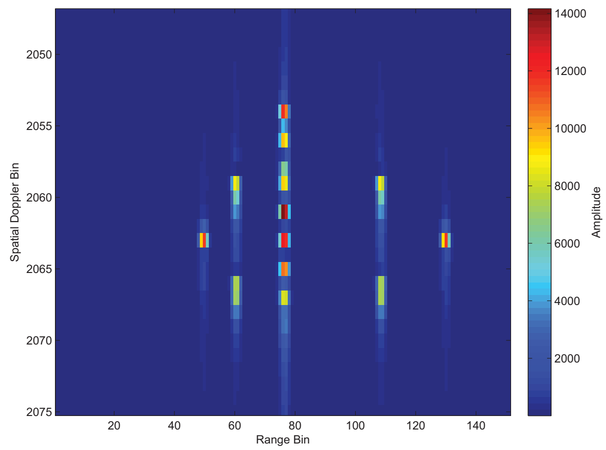


Figure 19: SAR image of a focused moving target after Linear Keystone imaging.

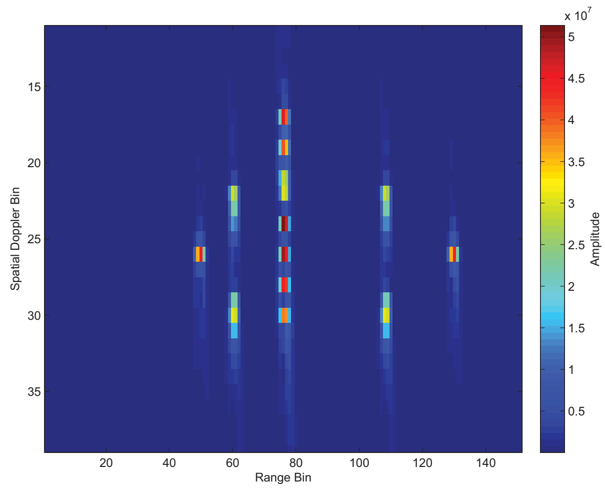


Figure 20: SAR image of a focused moving target after Second Order Keystone imaging.

also contains some residual smearing due to the same causes as those for the Linear Keystone based algorithm.

Figure 21 and Figure 22 show the variations, in the spatial Doppler domain, of the focused target responses for the two algorithms at a fixed range. These variations were obtained at the range bin containing the seven point targets of the composite target signature. Comparison of these two figures reveals the similarity of the results for the two Keystone based algorithms.

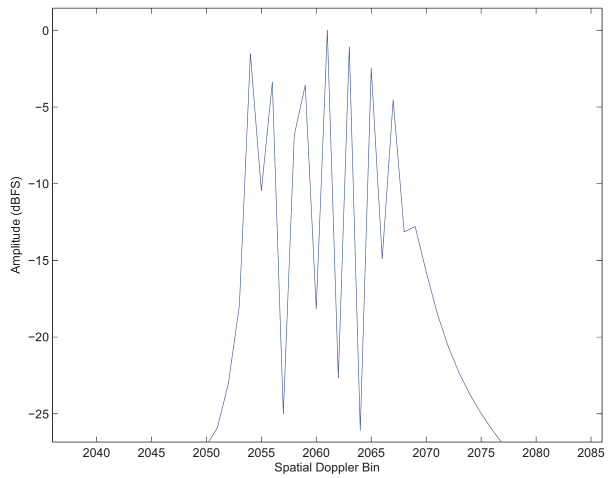


Figure 21: Amplitude response at a fixed range bin of the Linear Keystone image. Amplitude is dB Full Scale (dBFS).

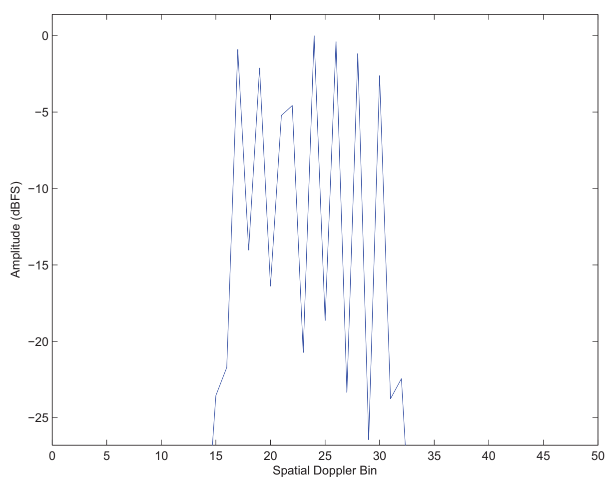


Figure 22: Amplitude response at a fixed range bin of the Second Order Keystone image. Amplitude is dB Full Scale (dBFS).

## 4.4 Imaging Results for Data from the XWEAR System

In this section, experimental results demonstrating the effectiveness of the previous algorithms are presented. The signal data were collected with DRDC's X-band Wideband Experimental Airborne Radar (XWEAR) system [7, 8]. The area being imaged is located in Ottawa, Ontario. The data set contains a moving target possessing a radial velocity, such that the resulting moving target signature is separated from the stationary background in the spatial Doppler frequency domain. This makes it possible to demonstrate the focusing algorithms with a realistic target while avoiding the complication of focusing a moving target "buried" in stationary clutter. Table 5 shows the parameters of the radar and the data collection geometry.

Figure 23 shows the range compressed data in the range/spatial Doppler domain. The moving target signature of interest has been highlighted within the figure. Figure 24 shows a zoomed view of the signature of the moving target. Due to the motion of the target, the signature displays both range walk and range curvature components which are easily recognizable. The radial velocity of the target results in the target signature being translated in the spatial Doppler dimension and the signature is separated from the stationary clutter.

Figure 25 illustrates the moving target signature after application of the Linear Keystone transform. The range walk component has been removed from the signature. However the signature still contains higher order range migration terms - mostly range curvature (quadratic). Figure 26 shows the focused moving target after application of the algorithm described in Section 4.1. Comparison of Figures 25 and 26 demonstrates the obtained cross-range compression. The residual smearing is believed to be due to uncompensated higher order motion components e.g. acceleration, jerk, and vibration.

Figure 27 illustrates the moving target signature after application of the Second Order Keystone transform. The range curvature (quadratic) component has been

Table 5: Radar Data Collection Parameters

| Symbol | Description | Value |
|---|---|---|
| PRF | Pulse Repetition Frequency | 1 KHz |
| $f_0$ | Radar Centre Frequency | 9.75 GHz |
| $R_c$ | Range to Scene Centre | 18.21 km |
| $\Delta r$ | Range Resolution | <1m |
| $\theta_c$ | Squint Angle | 24.74° |
| $v_p$ | Platform Velocity | 99 m/s |
| $L$ | Aperture Length | 407 m |
| $B_{az}$ | Azimuth Beamwidth | 2.4° |

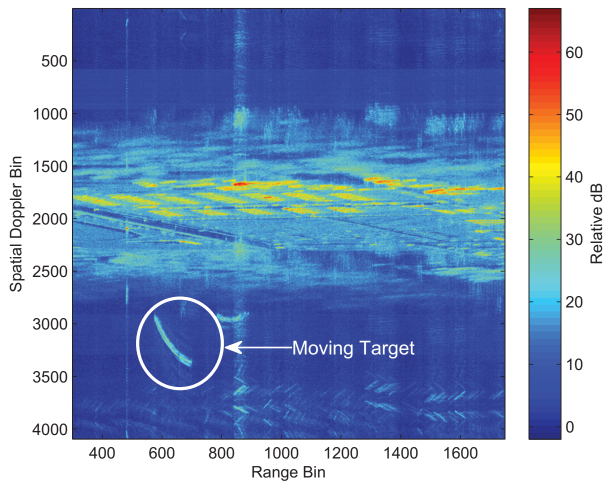


Figure 23: Full radar scene showing moving target signature in the range/spatial Doppler domain.

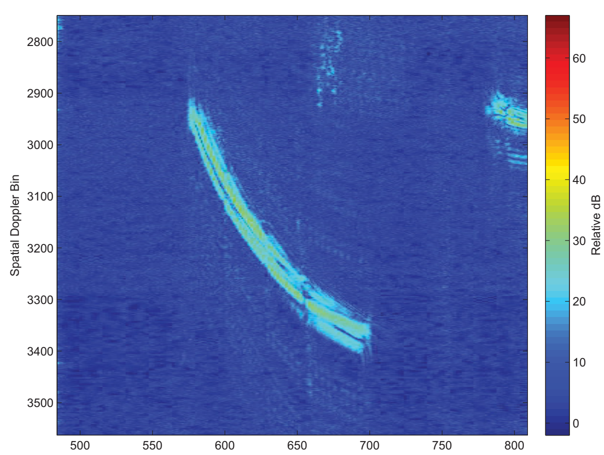


Figure 24: Moving target signature in the range/spatial Doppler domain.

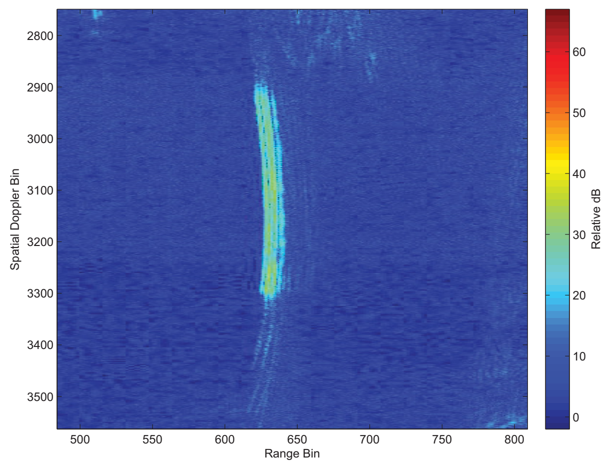


Figure 25: Moving target after Linear Keystone transform.

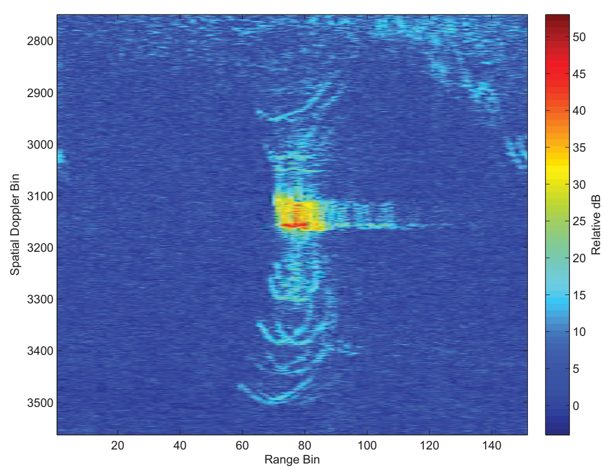


Figure 26: Moving target after applying the quadratic focusing step of the Linear keystone based algorithm.

removed from the signature, but linear and higher order range migration terms remain. Figure 28 shows the focused moving target after application of the algorithm described in Section 4.2. Comparison of Figure 27 and Figure 28 demonstrates the cross-range compression obtained with this algorithm. Comparison of the outputs of both Keystone based focusing algorithms i.e. Figure 26 and Figure 28, reveals that the algorithms produce similar results.

Figure 29 and Figure 30 show the variations, in the spatial Doppler domain, taken at a range bin of Figure 26 and Figure 28 respectively. The responses are quite similar in structure. Although the focused response of the moving target contains a strong peak, it also contains significant sidelobe structure caused by the uncompensated higher order phase terms.

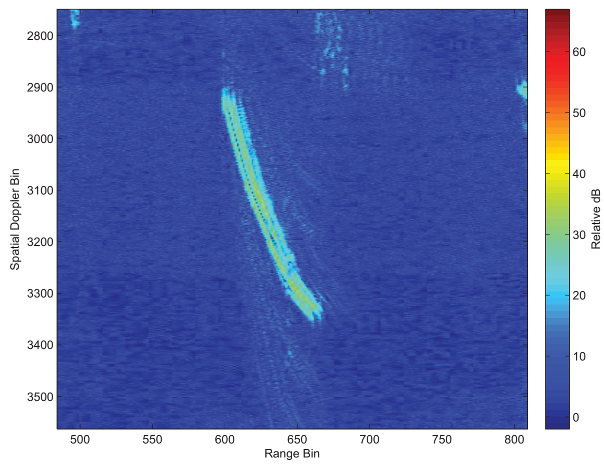


Figure 27: Moving target after Second Order Keystone transform.

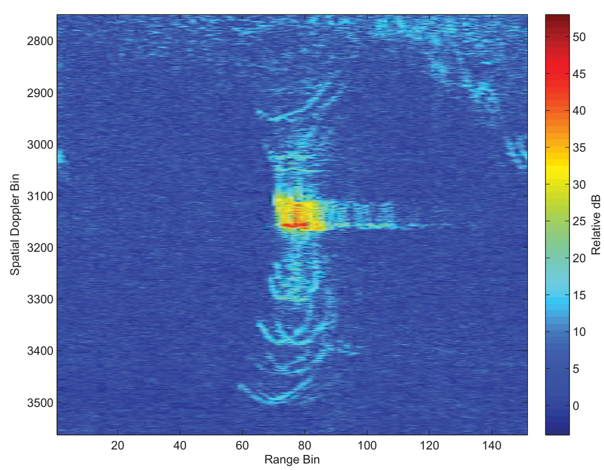


Figure 28: Moving target after applying the focusing step of the Second Order Keystone based algorithm.

Figure 31 shows the instantaneous phase response of the focused moving target taken at the same range bin used for Figure 29. The phase response was obtained by windowing around the moving target signature in Figure 26, applying an Inverse FFT in the spatial Doppler domain, and then calculating the phase of the result. Additionally, the linear portion of the phase response has been removed since it is not relevant to the focusing of the moving target signature. Analysis of the phase reveals the third and higher order phase components.

Figure 32 shows the magnitude response of the target corresponding to the range bin used in Figure 31. Figure 33 and Figure 34 show the phase responses at other range bins. Comparison of the three phase responses reveals their similarity. Data taken from the output of the Second Order Keystone based algorithm are nearly identical

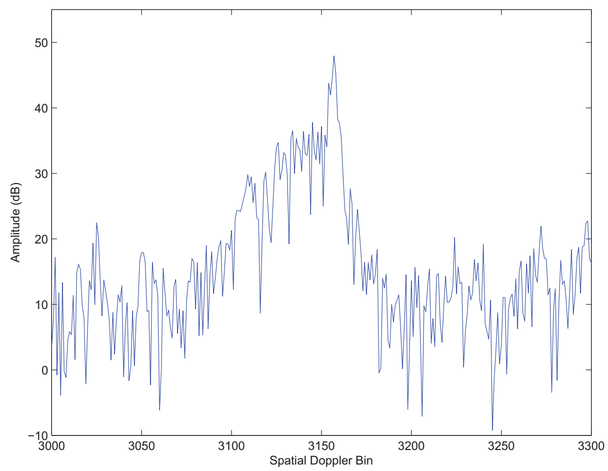


Figure 29: Moving target amplitude response from the Linear Keystone based algorithm. The response is taken at a fixed range bin.

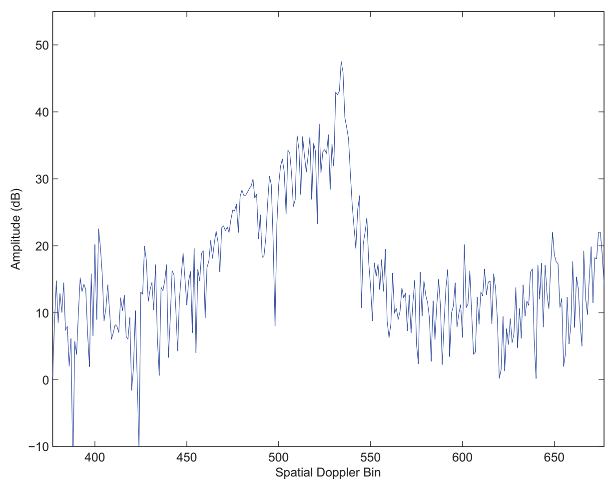


Figure 30: Moving target amplitude response from the Second Order Keystone based algorithm. The response is taken at the same range bin as used for Figure 29.

and therefore to avoid duplication they have not been included here.

To produce a highly focused image of the moving target would require appropriate compensation of the higher order phase terms. A study of such compensation techniques is beyond the scope of the current work, but is addressed in [5, 9]. For completeness, the magnitude responses of the target signature at the same range bins used in Figures 33 and 34 are shown in Figures 35 and 36 respectively.

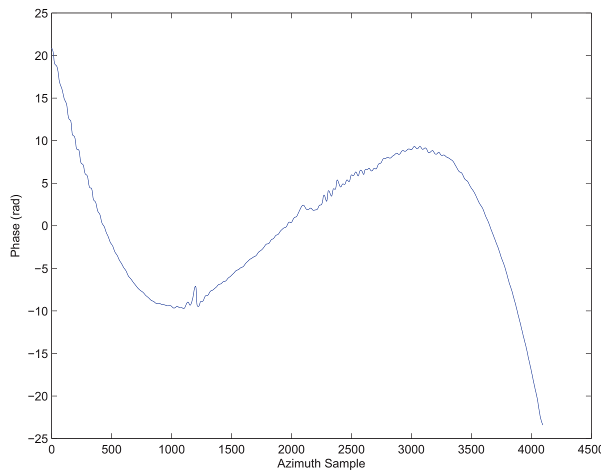


Figure 31: Unwrapped phase response (linear removal) of the focused target in the range/cross-range domain from the Linear Keystone base algorithm. The response is taken at the same range bin as used for Figure 29.

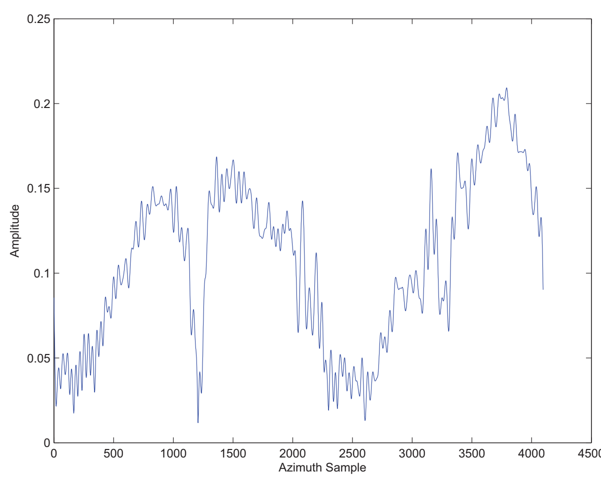


Figure 32: Amplitude response of target in the range/cross-range domain from the Linear Keystone base algorithm. The response is taken at the same range bin as used for Figure 29.

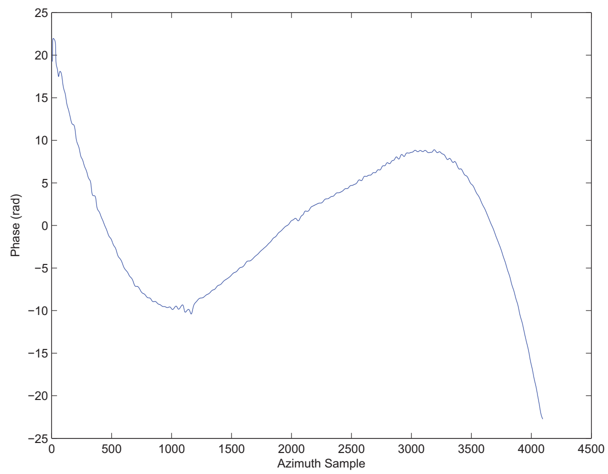


Figure 33: Unwrapped phase response (linear removal) of the focused target in the range/cross-range domain from the Linear Keystone base algorithm. The response is taken at a second range bin.

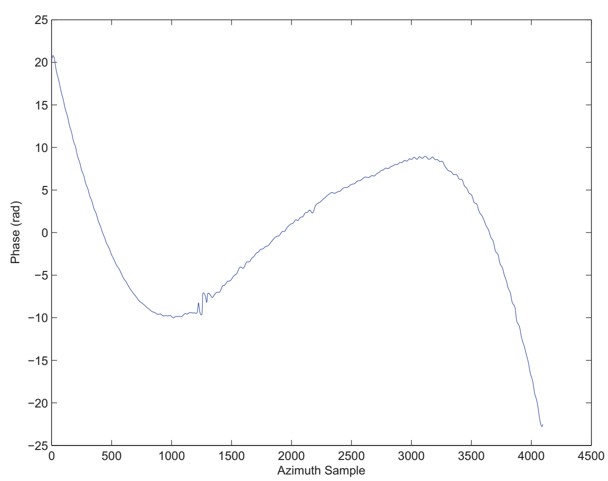


Figure 34: Unwrapped phase response (linear removal) of the focused target in the range/cross-range domain from the Linear Keystone base algorithm. The response is taken at a third range bin.

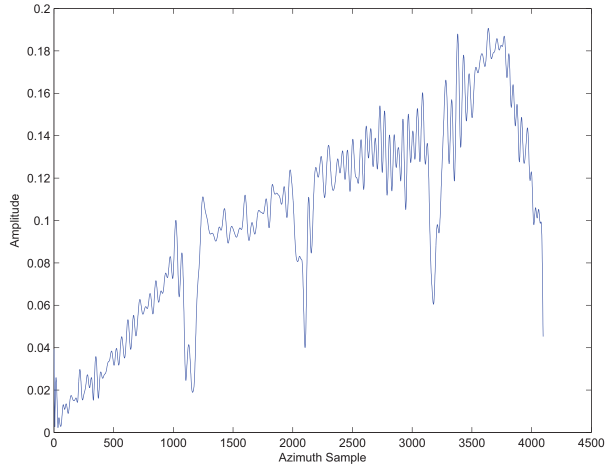


Figure 35: Amplitude response of target in the range/cross-range domain from the Linear Keystone base algorithm. The response is taken at the same range bin as used for Figure 33.

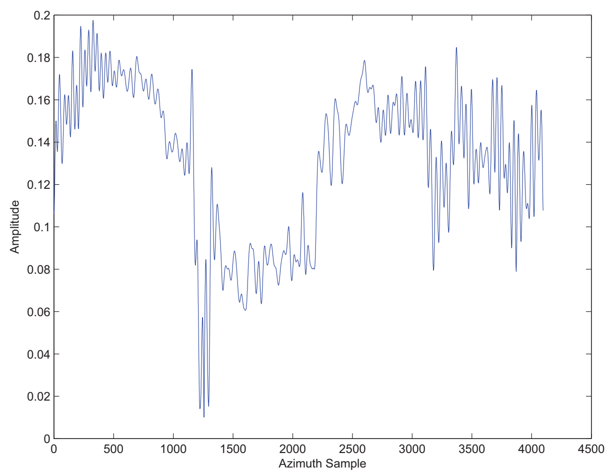


Figure 36: Amplitude response of target in the range/cross-range domain from the Linear Keystone base algorithm. The response is taken at the same range bin as used for Figure 34.

# 5 Conclusions

In this report the derivation of the Linear and Second Order Keystone transforms has been presented. The necessary sampling requirement for these transforms has been addressed. For the majority of radar systems with low fractional bandwidths, these sampling requirements are relatively modest if the original signal was sampled to meet the Nyquist criterion. Two methods were presented to address the situation when the radar target has a velocity and/or acceleration which causes the target signal to be subsampled. The first method involves applying a correction after application of the Keystone transform. However there are conditions limiting the applicability of this correction. The second algorithm provides a much more general solution. However the correction is applied before the Keystone transform and it is also necessary to search for an appropriate value of the offset velocity, $\dot{r}_c$. Unfortunately, the generality of the second approach results in increased computational complexity.

The effect of a moving target in Spotlight SAR data was analyzed and two algorithms were developed to focus the moving target signature. The first algorithm utilized the Linear Keystone transform, while the second algorithm was based on the Second Order Keystone transform. These algorithms were applied to both simulated SAR data and SAR data from the XWEAR system. The images obtained by applying these two algorithms are similar, but there is increased computational complexity for the algorithm using the Second Order Keystone transform. Thus, it appears that the algorithm utilizing the Linear Keystone transform would be preferred.

The Keystone based approaches to focusing moving target signatures in SAR data are capable of improving the coherent integration. Unfortunately for targets in realistic scenarios involving ground clutter, the resulting imagery is still of poor quality in comparison with standard imagery of stationary background. There are several reasons for this: the target has unknown motion components (e.g. acceleration, jerk, vibration and rotation), different components of the target may have different motion components, and the target signature is embedded in stationary clutter. For generating high resolution imagery it is necessary to have relatively long synthetic aperture times. In the case of airborne radar this may be on the order of hundreds of seconds. For a moving target in an urban environment, it is more likely for the target to undergo some form of acceleration or other higher order motion during this time. Further areas of investigation should involve the use of multiple channels to aid in clutter mitigation and techniques for addressing the higher order motion components.

# References


[1] Perry, R., DiPietro, R., and Fante, R. (1999), SAR Imaging of Moving Targets, *IEEE Transactions on Aerospace and Electronic Systems*, 35(1), 188–200.

[2] Zhou, F., Wu, R., and Bao, Z. (2007), Approach for single channel SAR ground moving target imaging and motion parameter estimation, *IET Radar, Sonar, and Navigation*, 1(1), 59–66.

[3] Raney, R. K. (1971), Synthetic Aperture Imaging Radar and Moving Targets, *IEEE Transactions on Aerospace and Electronic Systems*, 7(3), 499–505.

[4] Fienup, J. (2001), Detecting Moving Targets in SAR Imagery by Focusing, *IEEE Transactions on Aerospace and Electronic Systems*, 37(3), 794–808.

[5] Kirkland, D. (2011), Imaging Moving Targets Using the Second-Order Keystone Transform, *IET Radar Sonar and Navigation*, 5(8), 902–910.

[6] Soumekh, M. (1999), Synthetic Aperture Radar Signal Processing, First ed, John Wiley & Sons, Inc.

[7] Damini, A., McDonald, M., and Haslam, G. (2003), X-band Wideband Experimental Airborne Radar for SAR, GMTI and Maritime Surveillance, *IEE Proceedings Radar, Sonar and Navigation*, 150(4), 305–312.

[8] Damini, A., Balaji, M., Shafai, L., and Haslam, G. (2004), Novel Multiple Phase Centre Reflector Antenna for GMTI Radar, *IEE Proceedings Microwaves, Antennas and Propagation*, 151(3), 199–204.

[9] Kirkland, D. (2012), An Alternative Range Migration Correction Algorithm for Focusing Moving Targets, *Progress in Electromagnetics Research*, 131, 227–241.

This page intentionally left blank.

# Annex A: Derivation of $R_\Delta(u)$ Approximation

In order to determine the effects of the Linear and Second Order Keystone transforms, the phase in (48) needs to be expanded in a Taylor series in the cross range direction. Recall that the phase in (48) is given by

$$\phi(\omega, u) = -2(k + k_0) R_\Delta(u), \tag{A.1}$$

where

$$R_\Delta(u) = R(u) - R_{ref}(u), \tag{A.2}$$

$$R(u) = \left[(X_c + x_0 + v_x u)^2 + (Y_c + y_0 + v_y u - u)^2\right]^{\frac{1}{2}}, \tag{A.3}$$

and

$$R_{ref}(u) = \left[(X_c)^2 + (Y_c - u)^2\right]^{\frac{1}{2}}. \tag{A.4}$$

To simplify the calculation of the Taylor series, a binomial series expansion is first applied to $R_\Delta(u)$ w.r.t. the spatial variables $x_0 + v_x u$, and $y_0 + v_y u$. This leads to

$$R_\Delta(u) = \frac{X_c(x_0 + v_x u)}{R_{ref}(u)} + \frac{(Y_c - u)(y_0 + v_y u)}{R_{ref}(u)} + \ldots. \tag{A.5}$$

By ignoring higher order terms and defining the instantaneous squint angle $\theta(u) = \tan^{-1}\left(\frac{Y_c - u}{X_c}\right)$, $R_\Delta(u)$ can be written as

$$R_\Delta(u) = \cos\theta(u)(x_0 + v_x u) + \sin\theta(u)(y_0 + v_y u). \tag{A.6}$$

Using a narrow beamwidth approximation i.e. $u \ll \sqrt{X_c^2 + Y_c^2}$, $\theta(u)$ can be approximated by

$$\theta(u) \approx \theta_c - \frac{\cos\theta_c}{R_c} u, \tag{A.7}$$

where $R_c = \sqrt{X_c^2 + Y_c^2}$ and $\theta_c = \theta(0)$. Applying standard trigonometric relationships leads to the following approximations:

$$\begin{aligned} \sin\theta(u) &\approx \sin\theta_c - \frac{\cos^2\theta_c}{R_c} u, \\ \cos\theta(u) &\approx \cos\theta_c + \sin\theta_c \frac{\cos\theta_c}{R_c} u. \end{aligned} \tag{A.8}$$

Substituting the approximations of (A.8) in (A.6) gives

$$\begin{aligned} R_\Delta(u) \approx &\left(\cos\theta_c + \frac{\sin\theta_c \cos\theta_c}{R_c} u\right)(x_0 + v_x u) \\ &+ \left(\sin\theta_c - \frac{\cos^2\theta_c}{R_c} u\right)(y_0 + v_y u). \end{aligned} \tag{A.9}$$

This page intentionally left blank.

# Annex B: Phase Analysis in Squint Mode

In this section the phase response of the SAR signal in squint mode is analyzed. This derivation originally appeared in [5], but is included here for completeness. In squint mode (A.9) is in an inconvenient form. A rotated coordinate system can be utilized to simplify the expression for $R_\Delta(u)$ and result in a form that can be directly related to the zero squint condition. To simplify the analysis, it is useful to examine the impact of the rotated coordinates on the spatial components $(x_0, y_0)$ and the velocity components $(v_x, v_y)$ separately.

By rearranging terms, (A.9) can be rewritten as

$$\begin{aligned} R_\Delta(u) &= \left(\cos\theta_c + \frac{\sin\theta_c\cos\theta_c}{R_c}u\right)x_0 \\ &\quad + \left(\sin\theta_c - \frac{\cos^2\theta_c}{R_c}u\right)y_0 \\ &\quad + \left(\cos\theta_c + \frac{\sin\theta_c\cos\theta_c}{R_c}u\right)v_x u + \\ &\quad \left(\sin\theta_c - \frac{\cos^2\theta_c}{R_c}u\right)v_y u \\ &= R_1(u) + R_2(u), \end{aligned} \tag{B.1}$$

where

$$\begin{aligned} R_1(u) &= \left(\cos\theta_c + \frac{\sin\theta_c\cos\theta_c}{R_c}u\right)x_0 \\ &\quad + \left(\sin\theta_c - \frac{\cos^2\theta_c}{R_c}u\right)y_0, \end{aligned} \tag{B.2}$$

$$\begin{aligned} R_2(u) &= \left(\cos\theta_c + \frac{\sin\theta_c\cos\theta_c}{R_c}u\right)v_x u \\ &\quad + \left(\sin\theta_c - \frac{\cos^2\theta_c}{R_c}u\right)v_y u. \end{aligned} \tag{B.3}$$

(B.1) can be simplified by transforming to a rotated coordinate system. The rotated coordinates $(x', y')$ are defined as

$$\begin{bmatrix} x' \\ y' \end{bmatrix} = \begin{bmatrix} \cos\theta_c & \sin\theta_c \\ -\sin\theta_c & \cos\theta_c \end{bmatrix} \begin{bmatrix} x_0 \\ y_0 \end{bmatrix}. \tag{B.4}$$

Solving for $x_0$ and $y_0$ gives

$$\begin{bmatrix} x_0 \\ y_0 \end{bmatrix} = \begin{bmatrix} \cos\theta_c & -\sin\theta_c \\ \sin\theta_c & \cos\theta_c \end{bmatrix} \begin{bmatrix} x' \\ y' \end{bmatrix}. \tag{B.5}$$

Substituting (B.5) into (B.2) and simplifying gives

$$\begin{aligned} R_1(u) &= \left(\cos\theta_c + \frac{\sin\theta_c\cos\theta_c}{R_c}u\right)(x'\cos\theta_c - y'\sin\theta_c) \\ &\quad + \left(\sin\theta_c - \frac{\cos^2\theta_c}{R_c}u\right)(x'\sin\theta_c + y'\cos\theta_c) \\ &= x' - y'\frac{u\cos\theta_c}{R_c}(\sin^2\theta_c + \cos^2\theta_c) \\ &= x' - y'\frac{\cos\theta_c}{R_c}u. \end{aligned} \tag{B.6}$$

Similarly, the velocities will undergo the same rotational transformation as given in (B.5), that is

$$\begin{bmatrix} v_x \\ v_y \end{bmatrix} = \begin{bmatrix} \cos\theta_c & -\sin\theta_c \\ \sin\theta_c & \cos\theta_c \end{bmatrix} \begin{bmatrix} v'_x \\ v'_y \end{bmatrix}. \tag{B.7}$$

Substituting (B.7) into (B.3) gives

$$R_2(u) = v'_x u - v'_y\frac{\cos\theta_c}{R_c}u^2. \tag{B.8}$$

Substituting (B.6) and (B.8) into (B.1) gives

$$R_\Delta(u) = x' - \left(y'\frac{\cos\theta_c}{R_c} - v'_x\right)u - v'_y\frac{\cos\theta_c}{R_c}u^2. \tag{B.9}$$

The phase response of the SAR signal in squint mode can then be rewritten as

$$\begin{aligned} \phi(k,u) &= -2(k+k_0)R_\Delta(u) \\ &= -2(k+k_0)\left[x' - \left(y'\frac{\cos\theta_c}{R_c} - v'_x\right)u - v'_y\frac{\cos\theta_c}{R_c}u^2\right]. \end{aligned} \tag{B.10}$$

Comparing the phase in the squint mode geometry (B.10) with the phase from the broadside case (55), it is straightforward to see that squint mode operation can be treated as broadside mode operation by assuming a rotated geometry and scaling the resulting y axis variables (i.e $y'$, $v'_y$, etc.) by a factor of $\cos\theta_c$.

# Annex C: List of Symbols / Acronyms

| | |
|---|---|
| BW | Bandwidth |
| dB | Decibels |
| dBFS | Decibels Full Scale |
| DND | Department of National Defence |
| DRDC | Defence Research and Development Canada |
| DRDKIM | Director Research and Development Knowledge and Information Management |
| PRF | Pulse Repetition Frequency (Hz) |
| SAR | Synthetic Aperture Radar |
| $c$ | Speed of light in a vacuum (m/sec) |
| $f_0$ | Radar centre frequency (Hz) |
| $k$ | Temporal wavenumber (rad/m) |
| $k_0$ | Wavenumber of radar centre frequency $= \frac{2\pi f_0}{c}$ (rad/m) |
| $k_u$ | Spatial Doppler frequency (rad/m) |
| $k_{u\_BW}$ | Bandwidth in spatial Doppler frequency (rad/m) |
| $k_s$ | Spatial Doppler frequency sampling rate (rad/m) |

This page intentionally left blank.

**DOCUMENT CONTROL DATA**

(Security classif cation of title, body of abstract and indexing annotation must be entered when document is classif ed)

| | |
|---|---|
| 1. ORIGINATOR (The name and address of the organization preparing the document. Organizations for whom the document was prepared, e.g. Centre sponsoring a contractor's report, or tasking agency, are entered in section 8.)<br><br>Defence R&D Canada – Ottawa<br>3701 Carling Avenue, Ottawa ON K1A 0Z4, Canada | 2a. SECURITY CLASSIFICATION (Overall security classif cation of the document including special warning terms if applicable.)<br><br>UNCLASSIFIED<br><br>2b. CONTROLLED GOODS<br><br>(NON-CONTROLLED GOODS)<br>DMC A<br>REVIEW: GCEC JUNE 2010 |

3. TITLE (The complete document title as indicated on the title page. Its classif cation should be indicated by the appropriate abbreviation (S, C or U) in parentheses after the title.)

Linear and Second Order Keystone Transforms and Their Applications

4. AUTHORS (Last name, followed by initials – ranks, titles, etc. not to be used.)

Kirkland, D.

| | | |
|---|---|---|
| 5. DATE OF PUBLICATION (Month and year of publication of document.)<br><br>October 2013 | 6a. NO. OF PAGES (Total containing information. Include Annexes, Appendices, etc.)<br><br>62 | 6b. NO. OF REFS (Total cited in document.)<br><br>9 |

7. DESCRIPTIVE NOTES (The category of the document, e.g. technical report, technical note or memorandum. If appropriate, enter the type of report, e.g. interim, progress, summary, annual or f nal. Give the inclusive dates when a specif c reporting period is covered.)

Technical Memorandum

8. SPONSORING ACTIVITY (The name of the department project off ce or laboratory sponsoring the research and development – include address.)

Defence R&D Canada – Ottawa
3701 Carling Avenue, Ottawa ON K1A 0Z4, Canada

| | |
|---|---|
| 9a. PROJECT OR GRANT NO. (If appropriate, the applicable research and development project or grant number under which the document was written. Please specify whether project or grant.)<br><br>03mm | 9b. CONTRACT NO. (If appropriate, the applicable number under which the document was written.) |
| 10a. ORIGINATOR'S DOCUMENT NUMBER (The off cial document number by which the document is identif ed by the originating activity. This number must be unique to this document.)<br><br>DRDC Ottawa TM 2013-058 | 10b. OTHER DOCUMENT NO(s). (Any other numbers which may be assigned this document either by the originator or by the sponsor.) |

11. DOCUMENT AVAILABILITY (Any limitations on further dissemination of the document, other than those imposed by security classif cation.)

( X ) Unlimited distribution
(   ) Defence departments and defence contractors; further distribution only as approved
(   ) Defence departments and Canadian defence contractors; further distribution only as approved
(   ) Government departments and agencies; further distribution only as approved
(   ) Defence departments; further distribution only as approved
(   ) Other (please specify):

12. DOCUMENT ANNOUNCEMENT (Any limitation to the bibliographic announcement of this document. This will normally correspond to the Document Availability (11). However, where further distribution (beyond the audience specif ed in (11)) is possible, a wider announcement audience may be selected.)

UNLIMITED

13. ABSTRACT (A brief and factual summary of the document. It may also appear elsewhere in the body of the document itself. It is highly desirable that the abstract of classif ed documents be unclassif ed. Each paragraph of the abstract shall begin with an indication of the security classif cation of the information in the paragraph (unless the document itself is unclassif ed) represented as (S), (C), or (U). It is not necessary to include here abstracts in both off cial languages unless the text is bilingual.)

This report covers the basic theory of the First Order (Linear) and Second Order Keystone transforms. The associated sampling requirements are then derived and two compensation methods for handling subsampled systems are discussed. Linear and Second Order Keystone transforms are then applied to the problem of imaging moving targets in Synthetic Aperture Radar (SAR) systems for both simulated and acquired data. The results show that similar performance is achieved with both Keystone based algorithms.

14. KEYWORDS, DESCRIPTORS or IDENTIFIERS (Technically meaningful terms or short phrases that characterize a document and could be helpful in cataloguing the document. They should be selected so that no security classif cation is required. Identif ers, such as equipment model designation, trade name, military project code name, geographic location may also be included. If possible keywords should be selected from a published thesaurus. e.g. Thesaurus of Engineering and Scientif c Terms (TEST) and that thesaurus identif ed. If it is not possible to select indexing terms which are Unclassif ed, the classif cation of each should be indicated as with the title.)

SAR Imaging
Keystone Transform
Moving Target

**Defence R&D Canada**

Canada's leader in Defence
and National Security
Science and Technology

**R & D pour la défense Canada**

Chef de file au Canada en matière
de science et de technologie pour
la défense et la sécurité nationale

DEFENCE R&D DÉFENSE

www.drdc-rddc.gc.ca